

University of Virginia Forest Model Enhanced
Version 3 - August 2020

Technical Documentation

Adrianna Foster

August 21, 2020

Contents

1	Introduction	2
1.1	Model Structure	2
1.1.1	Scale and Spatial Interaction	4
2	Model Equations and Processes	6
2.1	Climate	6
2.1.1	Temperature, Precipitation, and Cloud Cover	6
2.1.2	Solar Radiation	11
2.1.3	Potential Evapotranspiration	20
2.2	Soil Processes	21
2.2.1	Soil Water	21
2.2.2	Soil Decomposition and Soil Nutrients	31
2.2.3	Permafrost	41
2.3	Moss	45
2.3.1	Moss Growth Factors	45
2.3.2	Moss Growth and Decay	46
2.4	Tree Growth	47
2.4.1	Tree Allometry	47
2.4.2	Growth Modifiers	51
2.4.3	Annual Growth	57
2.5	Tree Mortality	59
2.5.1	Growth Stress or Age	60
2.5.2	Disturbances	61
2.6	Tree Regeneration	70
2.6.1	Seed and Seedling Banks	71
2.6.2	Tree Establishment	72
2.7	Random Processes	73
2.7.1	Random Number Seeds	73
2.7.2	Pseudorandom Number Generators	74
References		78

Chapter 1

Introduction

1.1 Model Structure

The University of Virginia Forest Model Enhanced (UVAFME) is an update and extension of the individual-based gap model FAREAST (Yan & Shugart, 2005). As a traditional gap model, UVAFME simulates the establishment, growth, and mortality of individual trees on independent patches (i.e. plots) of a forested landscape (Fig. 1.1). The model is only spatially distributed in the vertical dimension, and plots are assumed to have no direct spatial interactions with one another. Through a Monte Carlo-style aggregation, the average of several hundred of these independent patches represents the average expected conditions of a forested landscape through time. As such, output from UVAFME is comparable to a statistically robust sampling of replicate forest inventory plots (Shugart & Woodward, 2011; Shugart et al., 2018).

Climate is based on input distributions of monthly precipitation, temperature, cloud cover, and relative humidity, derived from the historical data record. Daily soil moisture and nutrient dynamics are simulated based on a coupled, two-layer soil submodule using input site and soil characteristics.

Individual tree growth for each year is calculated through optimal diameter increment growth, modified by available resources and species- and tree size-specific tolerances to temperature and permafrost (if present), and light, moisture, and nutrient availability. Individual trees can thus compete with one another for above- and belowground resources. Light availability throughout the canopy is calculated using the Beer-Lambert Law and is dependent on the vertical distribution of leaf area within the plot. Tree growth response to temperature is based on an asymptotic relationship between growth rate and annual growing degree-days. Drought response is

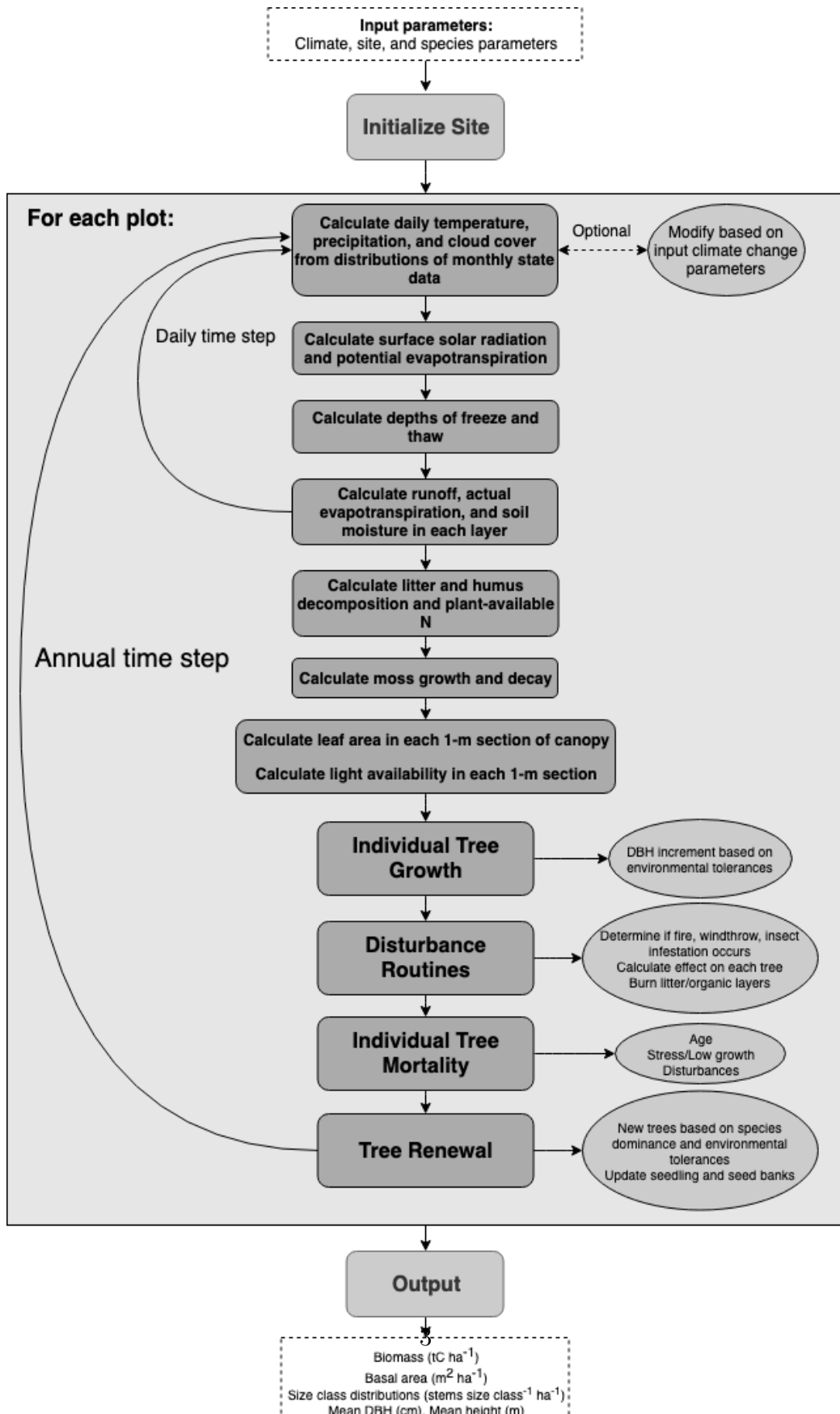


Figure 1.1: Main structure of UVAFME.

based on an index that represents the proportion of the growing season that experiences soil moisture limitation and/or high atmospheric demand. Nutrient availability response is based on responses to a relative nitrogen availability variable, calculated by comparing plant-available N (simulated in the decomposition subroutine) to the required N that year. The final annual increment growth for each tree is determined by multiplying the smallest (i.e. most limiting) growth-limiting factor by the optimal increment growth. Establishment of seedlings and saplings is based on species-specific resources and environmental tolerances as well as plot conditions.

Trees may die from age- or growth stress-related factors or by disturbances (i.e. fire, windthrow, or insect infestation). Fire and windthrow occurrence are probabilistic, based on site-specific mean return intervals. Fire and windthrow mortality are based on intensity (for fire), as well as species- and size-specific tolerances. Insect infestation is based on tree- and stand-level factors that increase probability of infestation and mortality. Trees that die, as well as annual leaf litter and woody debris are transferred to litter cohorts for decomposition.

1.1.1 Scale and Spatial Interaction

Currently, UVAFME sites do not interact with one another and thus may be run in parallel or in sequence. Within a site, several hundred (generally 200) independent plots about the area of influence of a dominant tree crown (e.g. 500 m²) are simulated that represent patches of a forested landscape (Fig. 1.2b). Forest “landscape” in this context is defined as a dynamic mosaic of forest gaps (i.e. patches/plots) (Shugart & Seagle, 1985). Within each patch, gap dynamics play out through the establishment of new trees following some major disturbance, growth and competition between trees to fill in the gap, eventual dominance or co-dominance of a few trees, and death of such canopy dominants, which starts the cycle anew (Fig. 1.2c) (Shugart, 1984). Within UVAFME, the plots do not interact with one another, and thus represent independent replicates of potential forest dynamics occurring at a location with input environmental and climatological conditions. Due to the stochastic factors within UVAFME (i.e. disturbances, mortality, and regeneration; see Sections 2.5 and 2.6), each plot represents a forest patch undergoing some gap dynamics process, driven by both deterministic processes (e.g. tree growth response to external factors; Section 2.4.2) and stochastic factors (e.g. mortality and disturbance events; Section 2.5). A Monte Carlo-style average of such plots thus represents average, non-spatially explicit (i.e. per area) *expected* forested conditions for the site location (Fig. 1.2d, e). This aggregation also produces emergent properties at the landscape scale

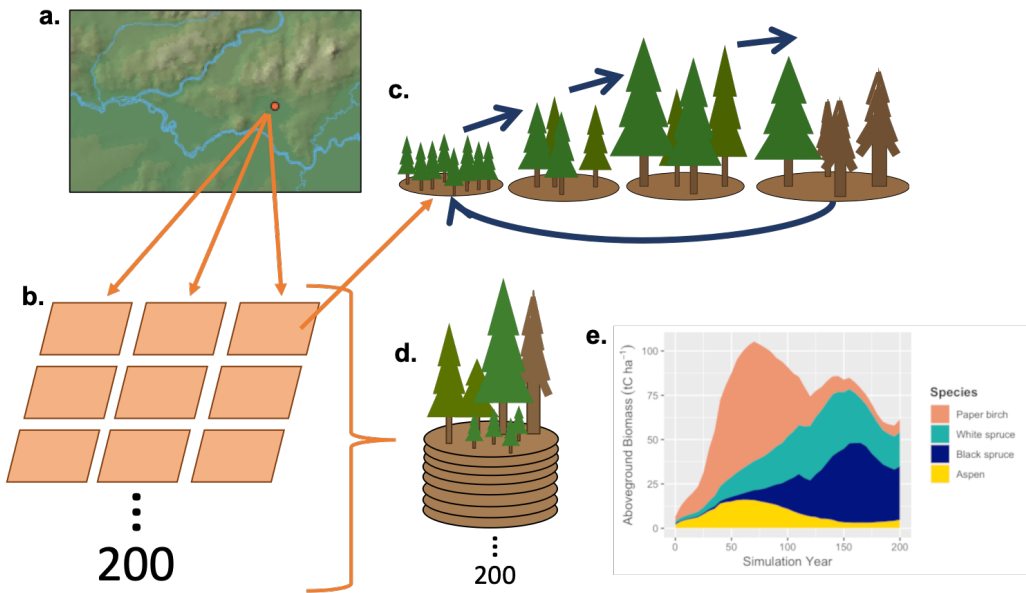


Figure 1.2: A single site simulated with UVAFME (a) contains several hundred independent plots (b), each undergoing independent gap dynamics processes (c). These plots are averaged together (d) to produce landscape-scale expected forested conditions over time, from bare-ground initiation and through forest succession (e).

(i.e. the average of several hundred gaps) such as forest succession (Fig. 1.2e), cyclical effects (Foster et al., 2015; Emanuel et al., 1978; Pastor et al., 1987), and response to shifting climate and disturbance regimes (Foster et al., 2017; Shuman et al., 2017; Shugart et al., 2018).

Climate and daily weather conditions in UVAFME are the same across all plots within a site, thus each plot experiences the same temperature, precipitation, cloud cover, and PET each simulation day. As of Version 3 of UVAFME, soil conditions within each plot are independent of one another, driven by the site-wide factors such as climate and input/initial soil conditions, as well as plot-specific factors such as forest cover and disturbances (Sections 2.2 and 2.5.2). Additionally, within each plot individual trees are placed on a 30×30 grid. Each plot is assumed to be horizontally (but not vertically) homogeneous with respect to canopy cover and leaf area, seed rain and seedling banks, as well as soil conditions.

Chapter 2

Model Equations and Processes

2.1 Climate

2.1.1 Temperature, Precipitation, and Cloud Cover

Climate in UVAFME is simulated through input distributions of monthly temperature ($^{\circ}\text{C}$), precipitation (cm), cloud cover (tenths of sky covered), and relative humidity (%). The average monthly minimum and maximum temperatures, precipitation, cloud cover, and relative humidity, as well as standard deviations for these values (generally derived from at least 30 years of historical climate data) are used to create a range of possible values for a site in question. Monthly and daily weather conditions are the same across all plots within a site.

Monthly Weather Values

The input distributions of climate variables are used to generate daily values of maximum temperature (t_{max}), minimum temperature (t_{min}), precipitation (p), cloudiness (c), and relative humidity (RH), throughout the simulation. For each year, the input mean monthly values are used to generate monthly values for that year using the variable's standard deviation and a normally distributed random number (mean = 0.0, sd = 1.0) between -1.0 and 1.0 for temperature, cloud cover, and humidity, and -0.5 and 0.5 for precipitation (see Section 2.7 on random processes):

$$t_m = \bar{t}_m + \bar{t}_{sd} t_f \quad (2.1.1)$$

$$p_m = \max(\bar{p}_m + \bar{p}_{sd} p_f, 0.0) \quad (2.1.2)$$

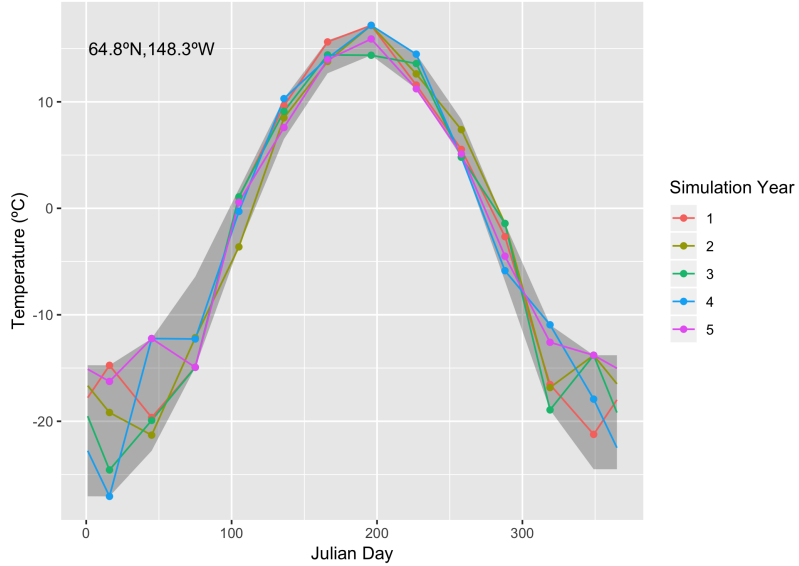


Figure 2.1: Example average monthly (points) and daily (lines) temperature ($^{\circ}\text{C}$) simulated by UVAFME for a site in interior Alaska. Shaded areas indicate the input mean \pm standard deviation.

$$c_m = \max (\bar{c}_m + \bar{c}_{sd} c_f, 0.0) \quad (2.1.3)$$

$$RH_m = \max (\bar{RH}_m + \bar{RH}_{sd} RH_f, 0.0) \quad (2.1.4)$$

where t_m is the monthly minimum or maximum temperature for a particular simulated month, \bar{t}_m and \bar{t}_{sd} are the input average and standard deviations of temperature (minimum or maximum) for that month, p_m is the monthly precipitation for a particular simulated month, \bar{p}_m and \bar{p}_{sd} are the input average and standard deviations of precipitation for that month, c_m is the monthly cloud cover for a particular simulated month, \bar{c}_m and \bar{c}_{sd} are the input average and standard deviations of cloud cover for that month, RH_m is the mean monthly relative humidity for a particular simulated month, \bar{RH}_m and \bar{RH}_{sd} are the input average and standard deviations of relative humidity for that month, and t_f , p_f , c_f , and RH_f are normally distributed random numbers, generated anew for each month of each year (see Section 2.7).

These monthly values are generated anew for each year of the simulation on each site and are equal across all plots within a site.

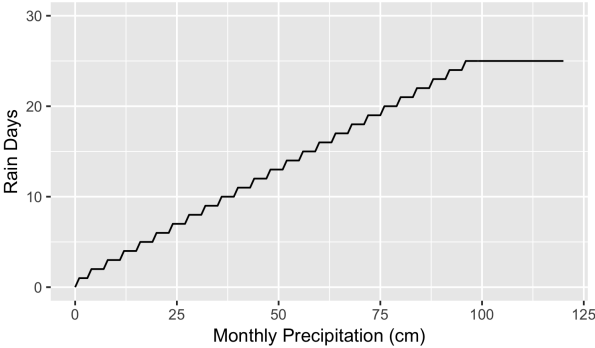


Figure 2.2: Number of rain days for a month based on monthly precipitation (cm) (Eq. 2.1.6).

Daily Weather Values

The monthly simulated weather data are used to generate daily values for each year using a Gaussian approach (Fig. 2.1). For temperature, cloud cover, and relative humidity, daily values are generated via:

$$v_d = v_m + \left(\frac{v_{m+1} - v_m}{j_{m+1} - j_m} \right) (j - j_m) \quad (2.1.5)$$

where v_d is the daily generated weather value (i.e. temperature, cloud cover, or relative humidity), v_m and v_{m+1} are the mean monthly value for the current and following months, j is the Julian day, and j_m and j_{m+1} are the Julian days corresponding to the middle of the current and following months. For days in December, monthly means from January of that year are used for the “following” month.

To generate daily precipitation values, the monthly precipitation is used to calculate the number of days it rains that month (Fig. 2.2), and the amount of rainfall for each rain day (Fig. 2.3). Rain days per month (d_r , Fig. 2.2) is calculated as:

$$d_r = \min \left(25, \frac{p_m}{4.0} + 1.0 \right) \quad (2.1.6)$$

Monthly rain days are distributed across the days in the month until all rain days have been used. Starting from the first of each month, if the number of rain days is greater than 0, a uniformly distributed random number between 0.0 and 1.0 is generated (u_r ; Section 2.7). If this number is less than or equal to the percent of rain days that month (i.e. $u_r \leq \frac{d_r}{d_m}$, where d_m is the number of days in the month), then the amount of rainfall for that day is set as $\frac{p_m}{d_r}$, otherwise no rainfall occurs that day. Once the number of rain

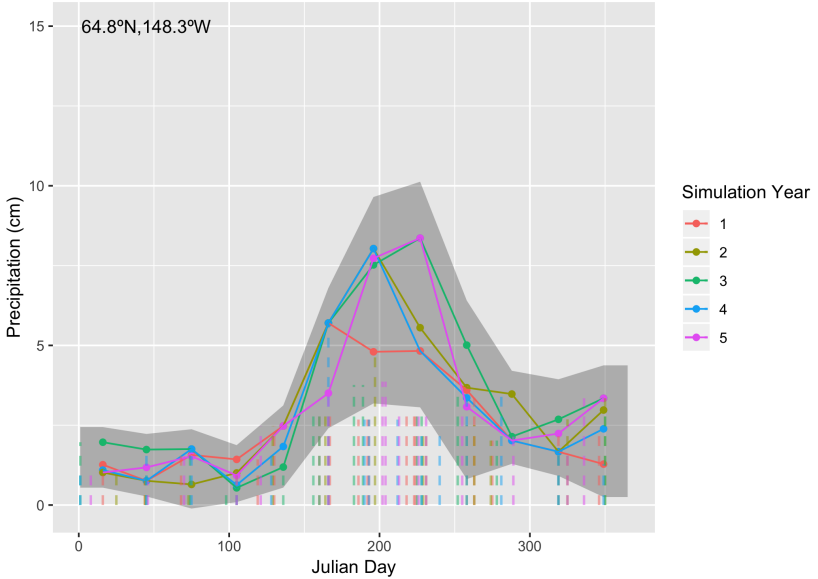


Figure 2.3: Example monthly (solid) and daily (dashed) precipitation (cm) simulated by UVAFME for a site in interior Alaska. Shaded areas indicate the input mean \pm standard deviation.

days in the month have been assigned, all subsequent days in the month have no rainfall.

Hourly Temperature Values

Hourly temperatures can also be calculated via a sinusoidal formula from (Reicosky et al., 1989). This formulation is based on daily minimum, maximum, and mean temperatures (t_{min} , t_{max} , and $t_{mean} = (t_{max} + t_{min})/2$) as well as sunrise hour (h_{rise}). Hourly temperature (t_h , °C) is calculated as:

$$t_h = \begin{cases} t_{mean} + \frac{t_{max}-t_{min}}{2} \cos\left(\frac{\pi(h+10)}{10+h_{rise}}\right), & 0 \leq h < h_{rise} \\ t_{mean} - \frac{t_{max}-t_{min}}{2} \cos\left(\frac{\pi(h-h_{rise})}{h_{max}-h_{rise}}\right), & h_{rise} \leq h \leq h_{max} \\ t_{mean} + \frac{t_{max}-t_{min}}{2} \cos\left(\frac{\pi(h+h_{max})}{10+h_{rise}}\right), & h_{max} < h \leq 24 \end{cases} \quad (2.1.7)$$

where h_{max} is the hour of maximum temperature, currently set to a default of 14 across all sites and year. Sunrise hour is calculated in the solar radiation subroutine (see Section 2.1.2) (Fig. 2.4).

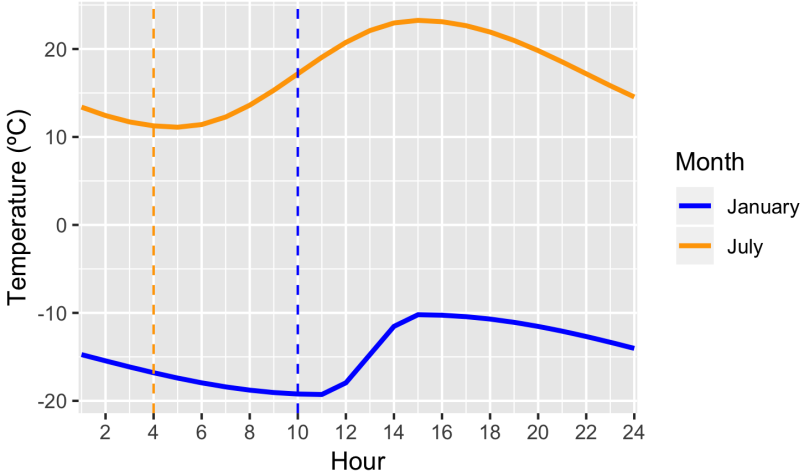


Figure 2.4: Example hourly temperature ($^{\circ}\text{C}$) for a site in interior Alaska on a typical day in mid-January ($t_{\min} = -19^{\circ}\text{C}$, $t_{\max} = -10^{\circ}\text{C}$) and mid-July ($t_{\min} = 11^{\circ}\text{C}$, $t_{\max} = 23^{\circ}\text{C}$). Dashed lines show time of sunrise.

Climate Change

Climate change can be prescribed either linearly or via an input climate change file. Climate change, in the form of changing mean monthly temperatures, precipitation, and relative humidity, is achieved by modifying the input values of average monthly minimum and maximum temperatures (\bar{t}_{\min} and \bar{t}_{\max}), precipitation (\bar{p}_m), and relative humidity (\bar{RH}_m) for a simulated site.

For linear climate change, total input temperature and/or precipitation change (t_c , $^{\circ}\text{C}$ or p_c , percent change, 0 to 1) is applied over an input duration (y_c , years) such that the amount of change per year is calculated as $t' = \frac{t_c}{y_c+1}$ and $p' = \frac{p_c}{y_c+1}$. Currently changes in relative humidity are only available via an input climate change file (see below).

When climate change starts in the model, the initial minimum and/or maximum temperatures are modified each year for the duration of the climate change application via $\bar{t}_m = \bar{t}_m + t'$. Likewise, the initial monthly precipitation values are modified each year for the duration of climate change application via $\bar{p}_m = \bar{p}_m + \bar{p}_m p'$. These modifications continue for the duration of climate change, at which point the total change in temperature or precipitation will have occurred, and all variables stabilize at the new values of $\bar{t}_m + t_c$ and $\bar{p}_m + \bar{p}_m p_c$.

For non-linear climate change simulations, new mean monthly values for each year are read in from an input climate change file.

Currently, all cloudiness variables and all monthly standard deviations do not change from the historical inputs during the climate change application.

Elevational Change

Often it is beneficial to run the model at the same site latitude and longitude, but at different elevations (such as in studies in complex terrain or for testing applications). Both temperature and precipitation change as altitude/elevation changes. These changes can be generated in UVAFME using input values of the base site elevation, the new elevation, and temperature and precipitation lapse rates. As with climate change, these modifications are made to the initial input average minimum and maximum temperatures and precipitation for a particular site. Temperature and precipitation are modified as:

$$\bar{t}_m = \bar{t}_m - 0.01(E' - E)t_l \quad (2.1.8)$$

$$\bar{p}_m = \max(\bar{p}_m + 0.001(E' - E)p_l, 0.0) \quad (2.1.9)$$

where E' is the new elevation at which the model is to be run (m), E is the original elevation at which the input climate data were derived (m), t_l is the input temperature lapse rate ($^{\circ}\text{C km}^{-1}$), and p_l is the input precipitation lapse rate (mm km^{-1}).

2.1.2 Solar Radiation

Daily and annual solar radiation is used to calculate potential evapotranspiration (PET) (Section 2.1.3) and permafrost dynamics (Section 2.2.3) within UVAFME. Previous versions of the model used top-of-atmosphere solar radiation to derive PET (Foster et al., 2017), however as of Version 3, surface solar radiation is used to account for the effects of slope, aspect, and cloud cover on solar radiation received at a surface (Fig. 2.5).

Top-of-Atmosphere Radiation

Top-of-atmosphere solar radiation ($\text{cal cm}^{-2} \text{ day}^{-1}$) is calculated as a function of latitude, solar declination, relative Earth-Sun distance, and sunrise/sunset hour angle (Brock, 1981). The eccentricity of Earth's orbit around the Sun causes the Earth-Sun distance to vary by $\sim 3\%$ throughout a single revolution (Brock, 1981) (Fig. 2.6). Such variation affects the amount of solar radiation received by the Earth throughout the year. The

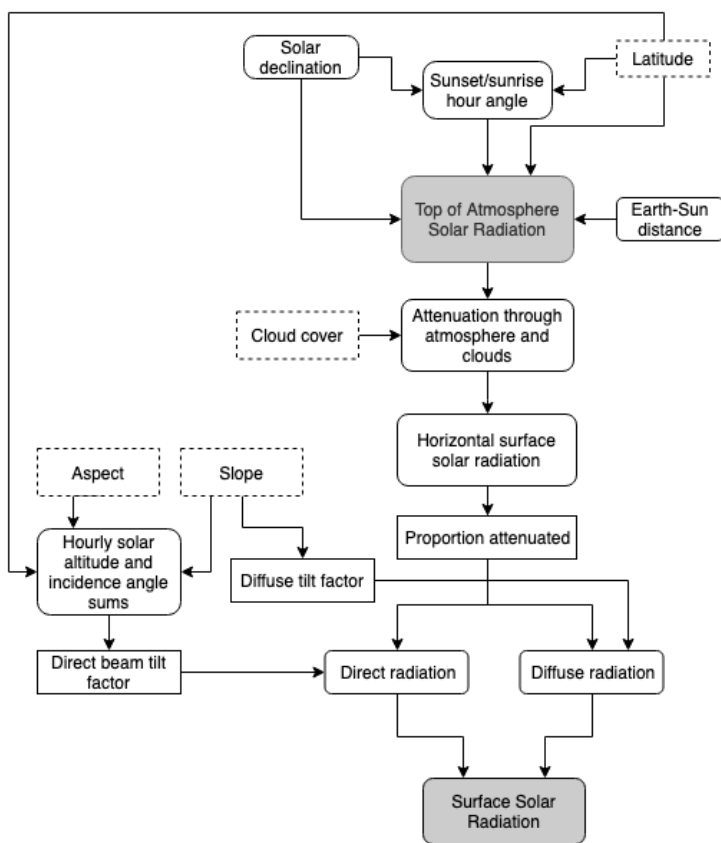


Figure 2.5: Flow diagram showing how solar radiation is calculated in UVAFME.

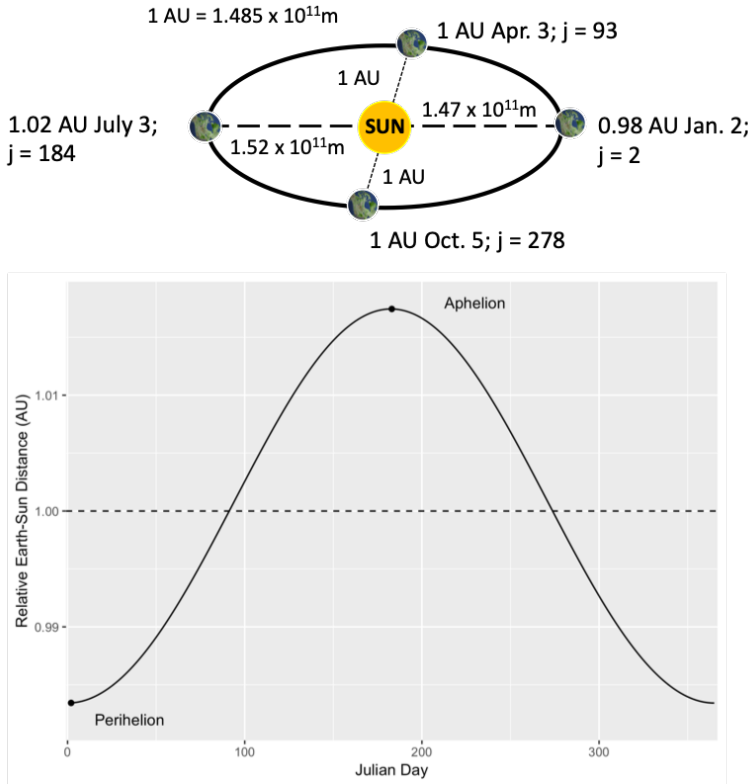


Figure 2.6: The Earth-Sun distance varies throughout the year due to the Earth's orbital eccentricity (Eq. 2.1.10)

relative Earth-Sun distance (r_{ES} , in AU; $1 \text{ AU} = 1.485 \times 10^{11} \text{ m}$) for day of year j can be calculated as (Brock, 1981; Nicholls & Child, 1979) (Fig. 2.6):

$$r_{ES} = \left(1.0 + 0.033 \cos(0.017214j) \right)^{-1/2} \quad (2.1.10)$$

Solar declination is the angular distance at solar noon between the Sun and the Equator (north-positive) and affects the solar radiation received at the top of the atmosphere. Earth is tilted at 23.4° from its plane of orbit. As the Earth revolves around the Sun, the solar declination changes such that at the spring and autumn equinoxes ($j = 80$ and 264) the Sun shines equally in both hemispheres and the declination is 0° . At the summer and winter solstices ($j = 173$ and 356) the Sun is directly overhead at 23.45°N and 23.45°S , respectively (Brock, 1981) (Fig. 2.7).

Solar declination (δ , radians) can be calculated using an equation from Cooper (1969):

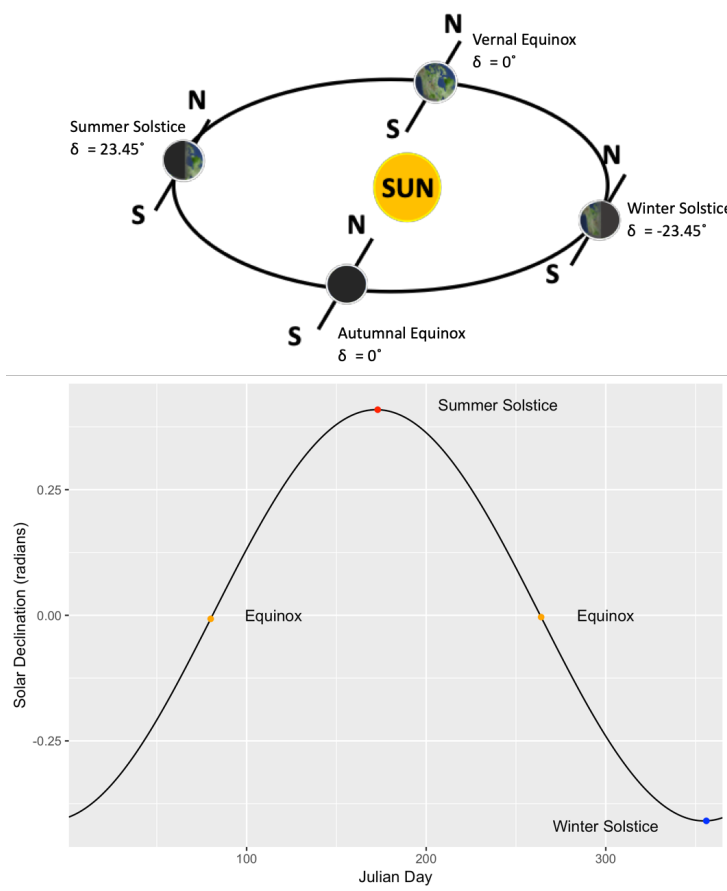


Figure 2.7: Declination varies throughout the year impacting top-of-atmosphere radiation (Eq. 2.1.11)

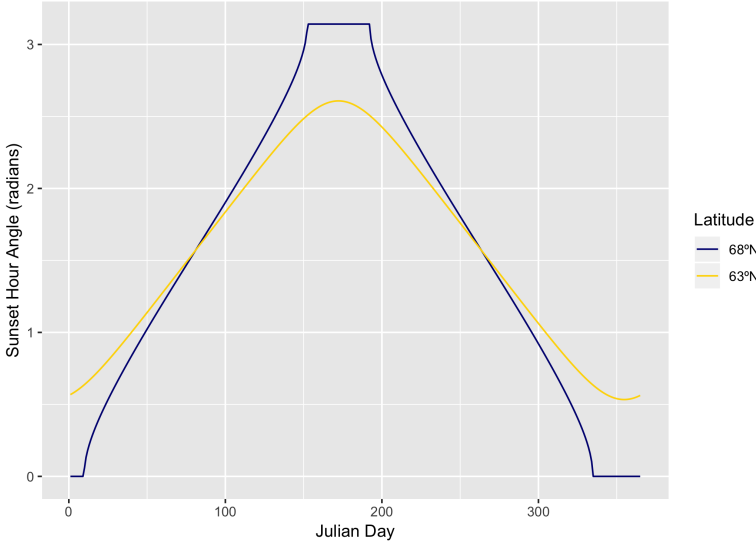


Figure 2.8: Example sunset hour angle calculation for two sites in interior Alaska (Eq. 2.1.12)

$$\delta = 23.45 \sin\left(\frac{284 + j}{365} 2\pi\right) \frac{\pi}{180} \quad (2.1.11)$$

Finally, sunset/sunrise hour angle is used to account for the daily rotation of Earth around itself. Sunset/sunrise hour-angle is the angle between the setting/rising Sun and the south point. This angle depends on declination as well as latitude on Earth, and can be calculated as (Brock, 1981) :

$$\cos \omega = -\tan \phi \tan \delta \quad (2.1.12)$$

where ω is the sunset/sunrise hour angle (radians), and ϕ is the site's latitude (radians). When $\tan \phi \tan \delta > 1.0$ the sun never sets, and the sunset/sunrise angle is set to π . When $\tan \phi \tan \delta < -1.0$ the sun never rises above the horizon and the sunset/sunrise angle is set to 0 (Keith & Kreider, 1978) (Fig. 2.8).

Top-of-atmosphere solar radiation is then calculated as (Klein, 1977):

$$R_{toa} = \frac{S}{\pi r_{ES}^2} \cos(\phi) \cos(\delta) \left(\sin(\omega) - \omega \cos(\omega) \right) \quad (2.1.13)$$

where R_{toa} is the solar radiation received at the top of the Earth's atmosphere ($\text{cal cm}^{-2} \text{ day}^{-1}$) and S is the solar constant ($2880 \text{ cal cm}^{-2} \text{ day}^{-1}$) (Fig. 2.9).

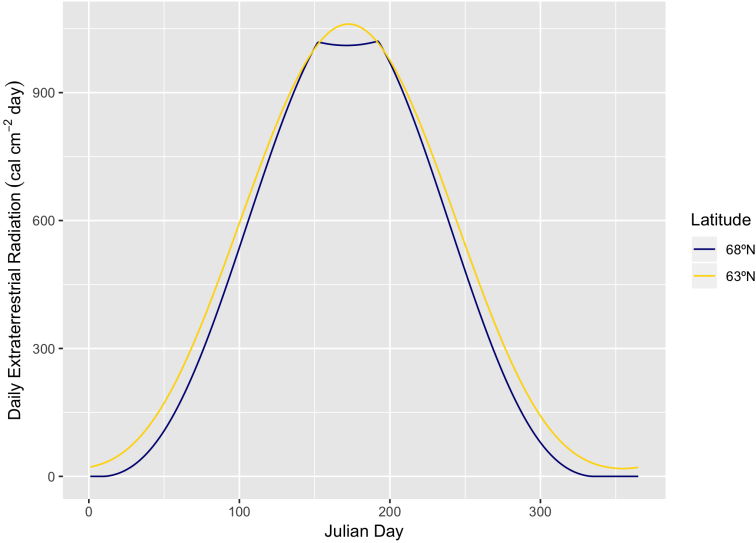


Figure 2.9: Example TOA solar radiation calculation for two sites in interior Alaska (Eq. 2.1.13)

Surface Radiation

Top-of-atmosphere solar radiation is first attenuated through the atmosphere and clouds using an equation from Bonan (1989) (Eq. 2.1.14). Bonan developed linear regressions of data from meteorological stations across North America, Scandinavia, and Russia on solar radiation and cloud cover (Fig. 2.10).

$$R_H = s_1 + s_2 R_{toa} - s_3 R_{toa}(c/10) \quad (2.1.14)$$

where R_H is surface solar radiation ($\text{cal cm}^{-2} \text{ day}^{-1}$) received on a horizontal surface, c is cloudiness (in tenths of sky covered), and s_1 , s_2 , and s_3 are parameters from Bonan (1989), with $s_1 = -7.130$, $s_2 = 0.812$, and $s_3 = 0.440$ for North America. This surface radiation is partitioned into direct and diffuse radiation using equations from Keith and Kreider (1978) (Fig. 2.11). Horizontal diffuse radiation (R_{Hd} , $\text{cal cm}^{-2} \text{ day}^{-1}$) is calculated as:

$$R_{Hd} = \begin{cases} \left(1.0045 + 0.04349K_t - 3.5227K_t^2 + 2.6313K_t^3\right)R_H, & K_t \leq 0.75. \\ 0.166R_H, & K_t > 0.75. \end{cases} \quad (2.1.15)$$

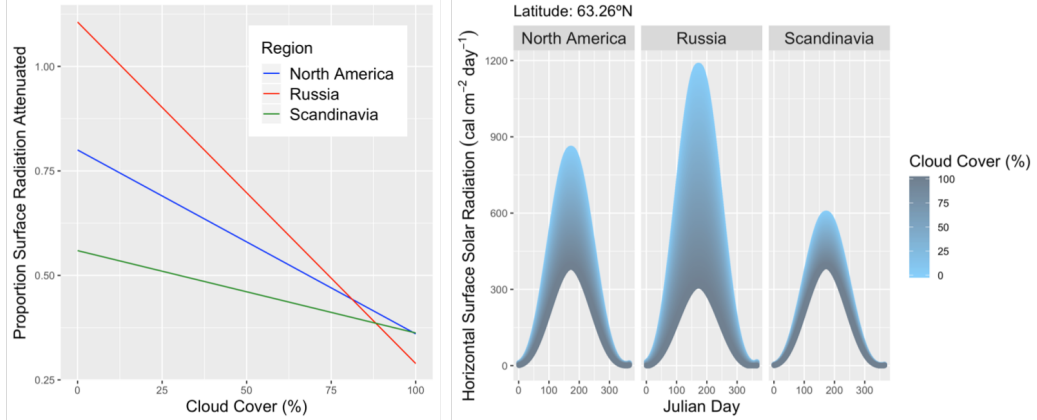


Figure 2.10: Left: linear regressions for attenuating top-of-atmosphere solar radiation through the atmosphere and clouds. Right: Example attenuated radiation at the same latitude for different levels of cloud cover for the three regions modeled in Bonan (1989) (Eq. 2.1.14).

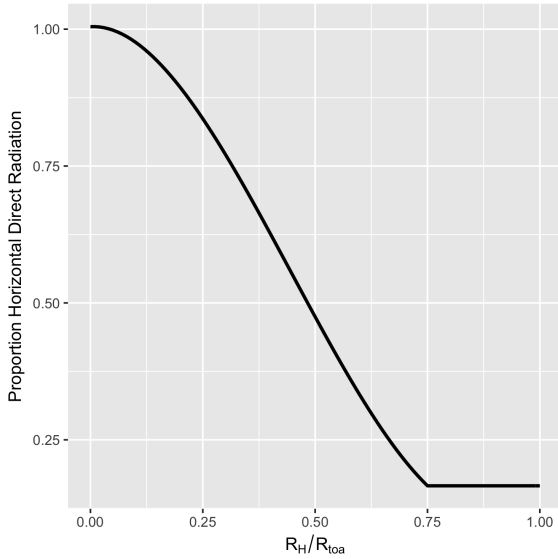


Figure 2.11: Relationship of fraction of TOA radiation attenuated by the atmosphere to direct radiation on a horizontal surface (Keith & Kreider, 1978) (Eq. 2.1.15).

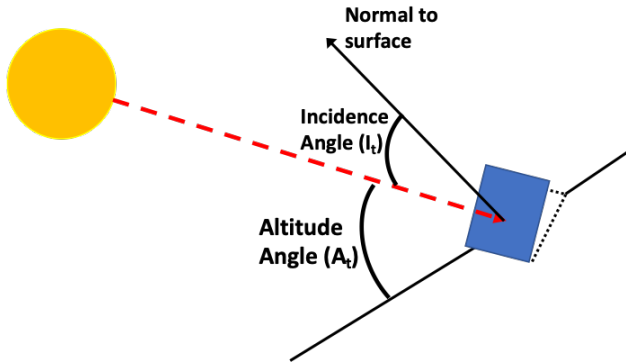


Figure 2.12: Solar altitude and incidence angles for a tilted surface.

where K_t is the fraction of top-of-atmosphere solar radiation attenuated by the atmosphere ($K_t = \frac{R_H}{R_{toa}}$). Horizontal direct beam radiation (R_{Hb} , cal cm^{-2} day $^{-1}$) is then calculated as:

$$R_{Hb} = R_H - R_{Hd} \quad (2.1.16)$$

Tilt factors, calculated using a site's slope and aspect, are used to convert horizontal surface diffuse and direct radiation into actual diffuse and direct radiation using equations from Bonan (1989) and Liu and Jordan (1962). The direct beam tilt factor is calculated using the daily sums of the cosine of hourly solar incidence angles and sine of hourly solar altitude angles.

For each day in the simulation, hourly solar altitude angles (A_t , radians) (i.e. altitude of the Sun relative to the Earth's horizon; Fig. 2.12) depend on latitude (ϕ , radians), solar declination (δ , radians), and the solar hour angle:

$$A_t = \arcsin \left(\sin(\phi) \sin(\delta) + \cos(\phi) \cos(\delta) \cos(h_s) \right) \quad (2.1.17)$$

where h_s is the solar hour angle (radians), calculated as $h_s = 15(12 - \frac{2t-1}{2})(\frac{\pi}{180})$, where t is hours from midnight. Hourly solar incidence angles (I_t , radians) (i.e. the angle at which the Sun's rays strike a surface; Fig. 2.12) are calculated using latitude, solar declination, solar hour angle, and surface orientation:

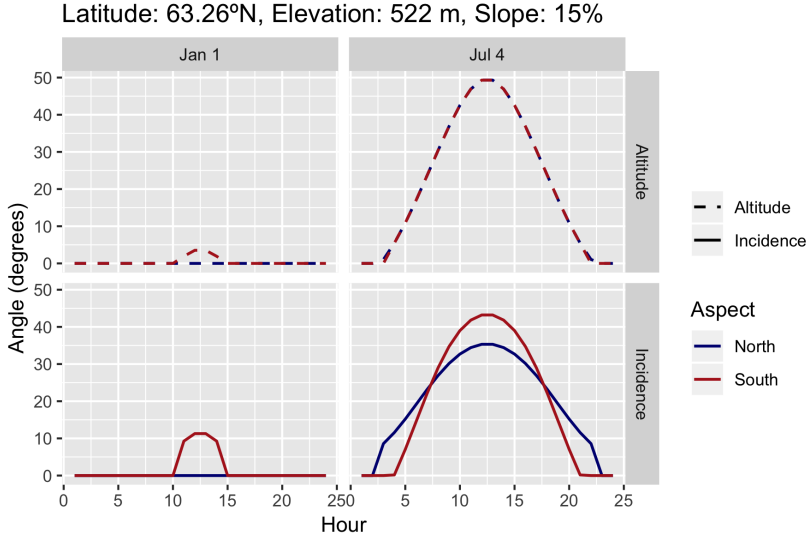


Figure 2.13: Calculation of hourly incidence and altitude angles for two days at north- and south-facing slopes in interior Alaska.

$$I_t = \arccos \left(\sin(\delta) \sin(\phi) \cos(z) - \sin(\delta) \cos(\phi) \sin(z) \cos(a_z) + \cos(\delta) \cos(h_s) \cos(\phi) \cos(z) + \cos(\delta) \cos(h_s) \sin(\phi) \sin(z) \cos(a_z) + \cos(\delta) \sin(z) \sin(a_z) \sin(h_s) \right) \quad (2.1.18)$$

where z is the slope of the site (radians) and a_z is the wall azimuth angle (radians), calculated as $a_z = (180 - a)(\frac{\pi}{180})$, where a is the site's aspect (degrees) (Fig. 2.13).

The cosine of hourly incidence and sine of hourly altitude angles are summed for each day to derive daily sums of altitude and incidence angles. It is assumed that the Sun is not above the horizon or in front of the surface when $A_t \leq 0^\circ$ or when $I_t \geq 90^\circ$. At these times, the angles are not added to the daily sums.

The direct beam tilt factor (F_b) is then calculated as:

$$F_b = \frac{I_{sum}}{A_{sum}} \quad (2.1.19)$$

where I_{sum} is the incidence angle sum, and A_{sum} is the altitude angle sum (radians). The diffuse radiation tilt factor (F_d) is calculated as:

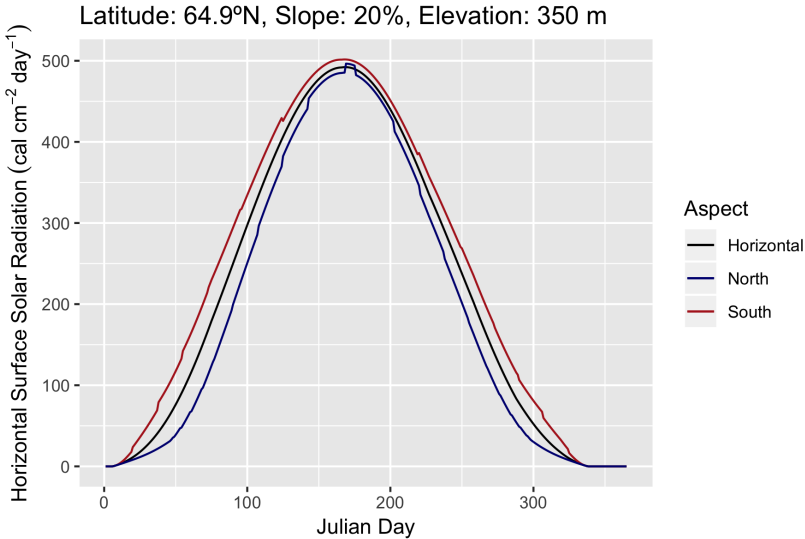


Figure 2.14: Example simulation of daily surface solar radiation ($\text{cal cm}^{-2} \text{ day}^{-1}$) for a location in interior Alaska with no slope and with 20% north- and south-facing slopes.

$$F_d = \left(\cos\left(\frac{z}{2}\right) \right)^2 \quad (2.1.20)$$

These tilt factors are used to calculate the diffuse, direct, and total solar radiation received at the surface ($\text{cal cm}^{-2} \text{ day}^{-1}$):

$$R = F_b R_{Hb} + F_d R_{Hd} \quad (2.1.21)$$

In this way, south-facing and north-facing slopes at the same latitude will receive different amounts of solar radiation throughout the year (Fig. 2.14), impacting the amount of PET and thus the site's moisture dynamics.

2.1.3 Potential Evapotranspiration

In previous versions of UVAFME, top-of-atmosphere radiation was used to calculate potential evapotranspiration (PET) using Hargreave's evaporation formula (Foster et al., 2017), however, studies have shown this equation to overestimate PET at high latitudes (Rosenberg et al., 1983; Bonan, 1989). In Version 3 of the model, the formulation for PET was updated to use a modified Priestley-Taylor equation as in Bonan (1989), which uses surface solar radiation, allowing for the incorporation of topographic effects on PET (Campbell, 1977):

$$PET = \begin{cases} \frac{a(t_{av}-b)R}{h_{vap}}, & t_{av} > 0. \\ 0 & t_{av} \leq 0. \end{cases} \quad (2.1.22)$$

where t_{av} is the mean daily temperature ($^{\circ}\text{C}$), h_{vap} is the latent heat of vaporization (kcal kg^{-1}), calculated as $h_{vap} = 597.391 - 0.5680t_{av}$, and a and b are site-specific coefficients, calculated using the average minimum and maximum daily temperatures of the warmest month of the year (Bosen, 1960):

$$a = \frac{1}{38 - \frac{2E}{305} + \frac{380}{e_2 - e_1}} \quad (2.1.23)$$

$$b = -2.5 - 0.14(e_2 - e_1) - \frac{E}{550} \quad (2.1.24)$$

where E is the site's elevation (m), and e_1 and e_2 are the saturation vapor pressures (mbar) at the mean minimum and maximum daily temperatures (t_m), respectively, of the warmest month of the year, calculated as:

$$e = 33.8639 \left((0.00738t_m + 0.8072)^8 - 0.000019|1.8t_m + 48| + 0.001316 \right) \quad (2.1.25)$$

Using this updated formulation, PET can differ between cold north-facing sites and warm south-facing sites (Fig. 2.15), impacting soil moisture and tree growth.

2.2 Soil Processes

2.2.1 Soil Water

Soil water balance in UVAFME is partitioned into two layers, a moss-organic layer containing a mixture of moss, humus, and litter, and a mineral (A) layer. Outputs are aggregated over the year to influence yearly tree growth (Section 2.4). Using this simple model allows for relatively little inputs: slope, canopy LAI, organic layer depth, drainage quality, soil texture, PET, and precipitation. These inputs are received from site input variables, the tree canopy module (Section 2.4.2), the soil nutrient submodel (Section 2.2.2), and the climate module (Section 2.1).

This updated version of UVAFME also allows for the incorporation of permafrost depth effects on soil moisture dynamics (Section 2.2.3). Each day in the simulation, soil moisture is partitioned into liquid and frozen water in

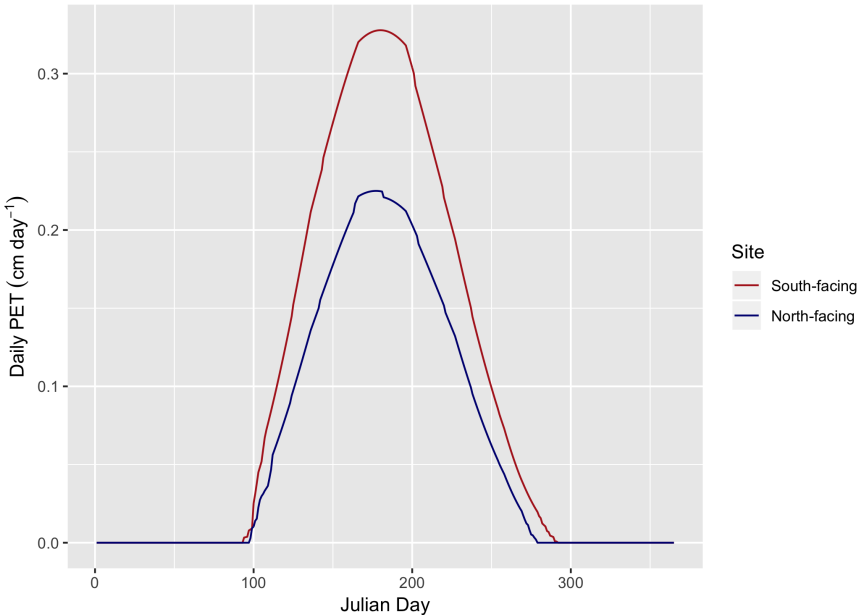


Figure 2.15: Example simulation of daily PET (cm day^{-1}) for a warm south-facing and a cold north-facing site in interior Alaska.

each soil layer, based on the calculation of depths of freezing and thawing in the permafrost submodel. As in Bonan (1989), for areas with continuous or discontinuous permafrost, it is assumed that the moss-organic and mineral layers are above field capacity at the beginning of each year (i.e. January 1, $jd = 1$). This effect of near-saturated conditions on moisture dynamics is implemented via drainage condition variables, which are set up at the beginning of each simulation year, based on the previous' years maximum depth of thaw (alt , m):

$$z_{\text{drain}} = \frac{m_{\text{sat}}(1 - alt) + m_{fc}(alt - 0.32)}{1 - 0.32} \quad (2.2.1)$$

where m_{sat} and m_{fc} are the saturation and field capacities of the soil layer (volumetric). These drainage parameters are corrected so that they are between the soil layer's field capacity and saturation capacity. The organic and mineral layer field capacity, saturation capacity, and wilting point for each site are set to default values as in Bonan (1989), based on the site's drainage class (i.e. well-, moderately, or poorly drained) (Table 2.1).

This drainage variable (z_{drain}) is used to modify the actual field and saturation capacities of soil (see below) and to calculate each soil layer's gravimetric moisture content at the beginning of the year as $gw = \frac{\rho_{\text{water}} z_{\text{drain}}}{bd_s}$,

Table 2.1: Input soil parameters (volumetric). Values taken from Bonan (1989).

Soil Layer	Variable	Well drained	Moderately drained	Poorly drained
organic	saturation capacity	0.39	0.39	0.39
	field capacity	0.39	0.39	0.39
	permanent wilting point	0.039	0.039	0.039
mineral (A-layer)	saturation capacity	0.35	0.44	0.53
	field capacity	0.20	0.29	0.38
	permanent wilting point	0.06	0.06	0.06

where bd_s is the soil layer's bulk density, set to 85 kg m^{-3} for the organic layer and 1250 kg m^{-3} for the mineral layer (Bonan, 1989). Additionally, it is assumed that all soil moisture at the beginning of the year is frozen (i.e. $w_i = z_{drain}d_s$ and $w_l = 0.0$, where w_i and w_l are the amounts of frozen and liquid water, respectively in the soil layer (m), and d_s is the depth of the soil layer (m)).

Soil Moisture Dynamics

The amount of soil moisture (liquid and frozen) is updated on a daily time step, incorporating effects from precipitation, canopy interception, runoff, snowpack melt, soil freezing and thawing, soil water infiltration, and evaporation (Fig. 2.16).

Precipitation (input from the climate module) is initially received at the surface. As in previous versions of UVAFME, precipitation is partitioned into liquid rainfall and snow, depending on temperature. In this updated version, a new equation was used for simulating a mixture of snow and rain when the air temperature is near freezing. If the mean daily temperature is greater than or equal to 3.3°C , all precipitation is assumed to be liquid rainfall. If t_{av} is at or below -1.1°C , all precipitation is assumed to be snow. If t_{av} is between 3.3°C and -1.1°C , precipitation is assumed to be a mixture of snow and liquid water, with the portion that falls as snow calculated as (Wigmsta et al., 1994):

$$P_{snow} = \frac{(3.3 - t_{av})}{(3.3 - -1.1)} P \quad (2.2.2)$$

where P is total precipitation (m) and P_{snow} is snowfall in snow-water-equivalent (m). All snowfall is then accumulated in an annual snowpack and snow-water equivalent (SWE) bank. Canopy interception (I , m) from liquid rainfall is calculated as:

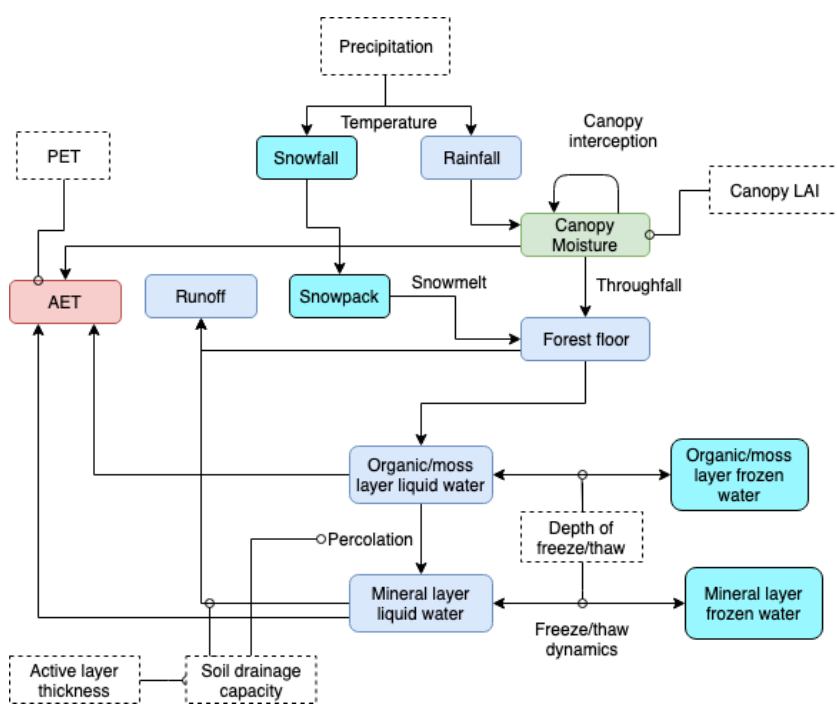


Figure 2.16: Flow diagram showing moisture dynamics simulated in UVAFME.

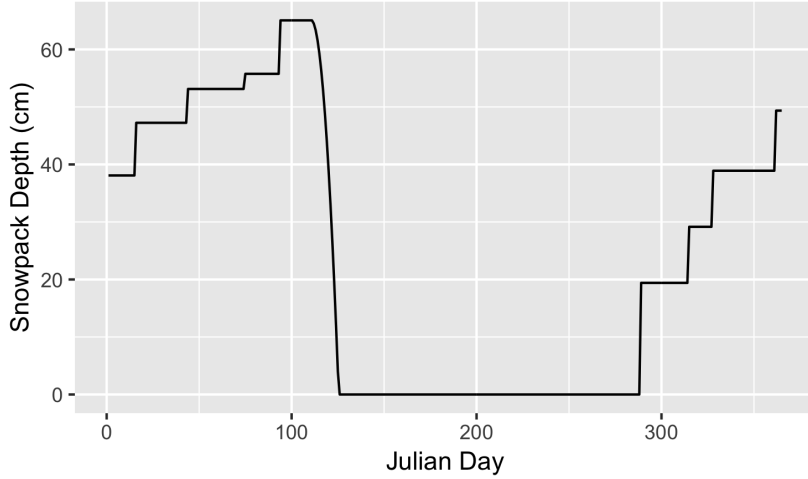


Figure 2.17: Example simulation of snowpack accumulation and melt (cm day^{-1}) for a site in interior Alaska.

$$I = \min \left(\max(laiw_{max} - laiw, 0.0), P_{rain} \right) \quad (2.2.3)$$

where $laiw_{max}$ is the maximum water content of the canopy (m), calculated as $0.0015LAI$, and $laiw$ is the current water content of the canopy (m). Throughfall is then calculated as $t_{fall} = \max(P_{rain} - I, 0.0)$, and the water content of the canopy is increased by the interception amount.

When there is snow on the ground and the air temperature is above freezing, the snowpack melt amount (m) is calculated using the degree method (Singh et al., 2000):

$$s_{melt} = 0.001 \left(c_m(t_{av} - t_c) \right) \quad (2.2.4)$$

where c_m is a site-specific coefficient, set to 4.0 for forested sites (DeWalle et al., 2002), and t_c is the critical freezing temperature, set to 0.0°C . The snow-water equivalent bank is then decreased by the snowmelt amount, and the snowpack depth is updated as:

$$d_{snow} = \frac{swe}{\frac{\rho_{snow}}{\rho_w}} \quad (2.2.5)$$

where swe is snow-water equivalent (m), ρ_{snow} is the density of snow, set to 217 kg m^{-3} (Sturm et al., 2010), and ρ_w is the density of water (1000 kg m^{-3}) (Fig. 2.17).

Slope runoff is then calculated as:

$$R_s = \left(\frac{\theta}{90}\right)^2 t_{fall} \quad (2.2.6)$$

where θ is the slope of the site (degrees). Potential water loss or gain for the simulation day is calculated as:

$$pw = t_{fall} + s_{melt} - R_s - PET \quad (2.2.7)$$

In this updated version of UVAFME, the amount of water that freezes and thaws each day is also calculated based on Bonan (1989) and incorporated into the soil moisture dynamics. For each soil layer (i.e. the moss-organic and mineral layers), the amount of water released in soil thawing (w_t , m) is calculated as a proportion of the change in depth of thaw from the previous day to the current simulation day:

$$w_t = \min\left(z_{drain}(d_{thaw} - d'_{thaw}), w_i\right) \quad (2.2.8)$$

where d_{thaw} is the depth of thaw in that layer (see Section 2.2.3) on the current day (m), d'_{thaw} is the depth of thaw from the previous day (m), and w_i is the ice content of that layer (m). This amount is subtracted from the ice water content of the soil layer and added to the liquid water content. The depth of thaw is also used to update that layer's saturation capacity, field capacity, and wilting point:

$$m'_{sat} = m_{sat}d_{thaw} \quad (2.2.9)$$

$$m'_{fc} = m_{fc}d_{thaw} \quad (2.2.10)$$

$$m'_{pwp} = m_{pwp}d_{thaw} \quad (2.2.11)$$

After the soil thawing is accounted for, if there is a positive water balance from precipitation (i.e. $pw \geq 0.0$ from Eq. 2.2.7), actual evapotranspiration (AET , m) is set equal to PET, and the positive water balance is added to the organic-moss layer, adjusting for excess water from infiltration and thawing. Excess water ($w_{exs} = \max(w_l - m_{fc}, 0.0)$, in m) within a layer is removed using a modified equation from Botkin (1993). This formulation assumes that as rainfall/water input intensity increases or as the soil layer becomes more saturated, the amount of runoff/soil percolation increases (Fig. 2.18). The proportion of excess water that runs off or percolates to a lower layer is calculated as:

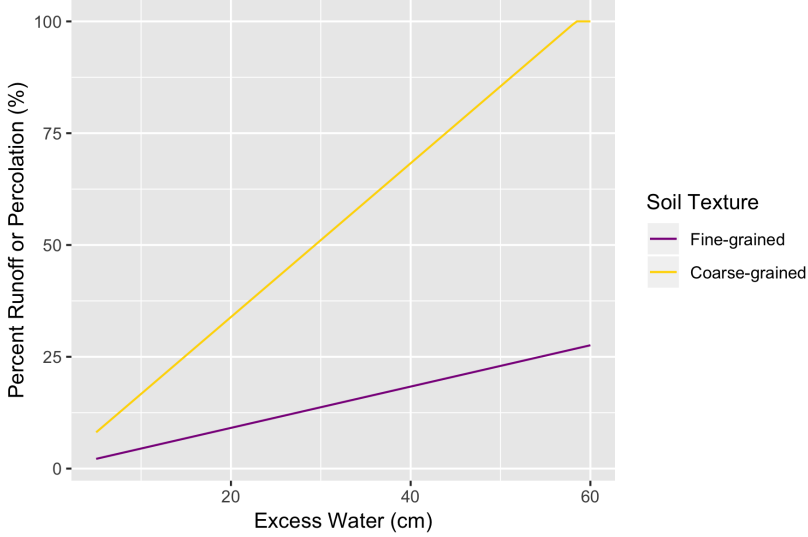


Figure 2.18: Example calculation of fraction of excess water (above field capacity) that runs off or percolates to a lower soil layer for a coarse-grained and fine-grained soil with PET = 0.3 cm day⁻¹ (Eq. 2.2.12).

$$f_{exs} = b \left(\frac{w_{exs}^2}{PET + w_{exs}} \right) \left(1 - (m_{fc} - m_{pwp}) \right) \quad (2.2.12)$$

where b is based on soil texture and is set to 2.0 for coarse-grained soils and 0.6 for fine-grained soils. Excess water is then subtracted from the soil layer as:

$$w_l = w_l - w_{exs} f_{exs} \quad (2.2.13)$$

The excess water from the moss-organic layer is transferred to the mineral layer, and excess water from the mineral layer is calculated and subtracted (Fig. 2.19, 2.20).

If there is a negative water balance due to high PET or low moisture inputs (i.e. $pw < 0.0$, from Eq. 2.2.7), evaporation from the canopy and both soil layers occurs. Canopy evaporation (E_{can} , m) is calculated as:

$$E_{can} = \min \left(-pw, \max(laiw - laiw_{min}, 0.0) \right) \quad (2.2.14)$$

where $laiw_{min}$ is the minimum water content of the canopy (m), calculated as $1.0 \times 10^{-4} LAI$. This evaporation amount is subtracted from the canopy water content, and pw is increased (i.e. made less negative) to account for canopy evaporation:

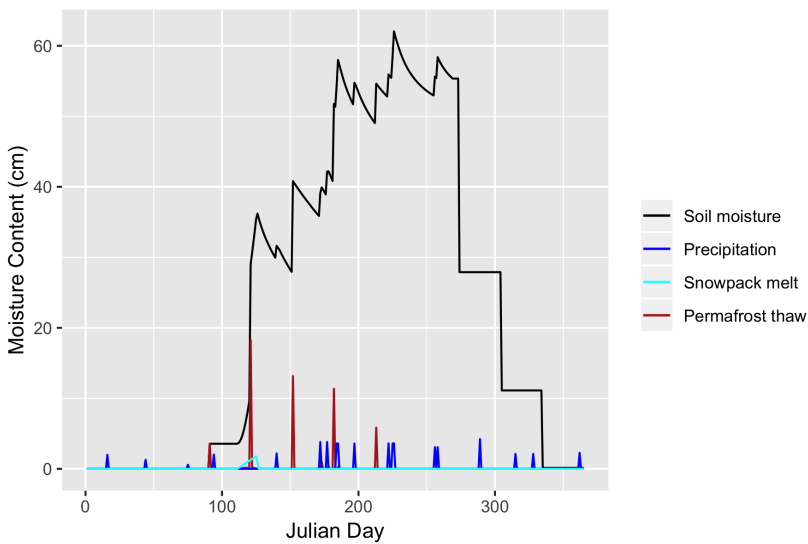


Figure 2.19: Example simulation of liquid soil moisture (cm) throughout the year for a site in interior Alaska. Dark blue lines indicate precipitation inputs, red lines indicate water from soil thawing, and cyan lines indicate water from snowpack melt.

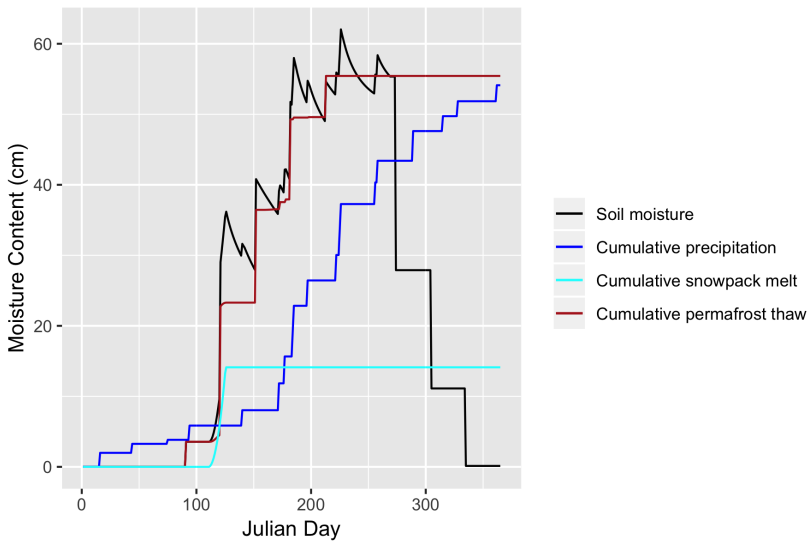


Figure 2.20: Example simulation of liquid soil moisture (cm) throughout the year for a site in interior Alaska. Dark blue lines indicate cumulative precipitation inputs, red lines indicate cumulative permafrost thaw, and cyan lines indicate cumulative snowpack melt.

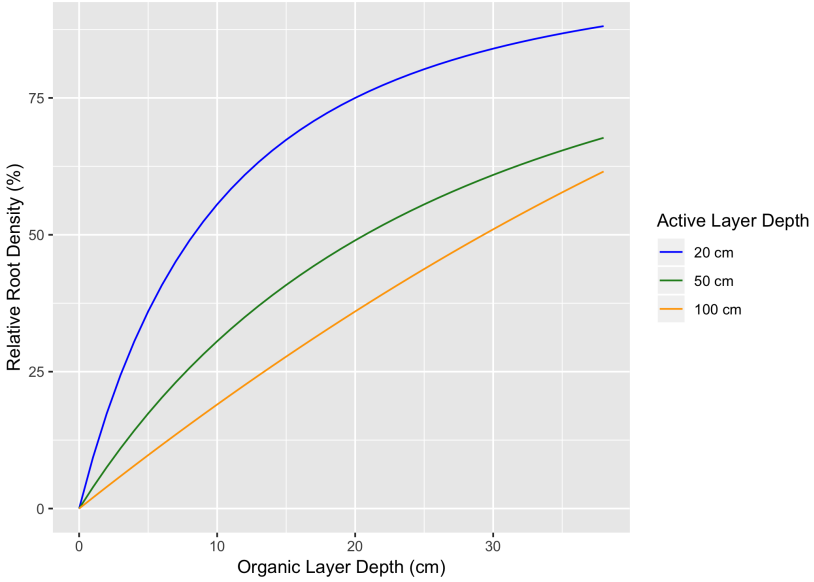


Figure 2.21: Relative root density in the organic layer with changing organic layer and active layer depths (Eq. 2.2.16).

$$pw = \min(pw + E_{can}, 0.0) \quad (2.2.15)$$

If pw is still negative, and there is at least some amount of unfrozen soil moisture (i.e. $d_{thaw} > 0.0$), evaporation occurs from the soil layers. The amount lost from each layer is dependent on the relative root distribution of each layer. As in Bonan (1989), the relative root distribution (r_z) for the organic layer is calculated as:

$$r_z = \left(\frac{2d_{org}}{\min(d_{org} + alt, 1.0)} \right) \left(1 - \frac{d_{org}}{2(\min(d_{org} + alt, 1.0))} \right) \quad (2.2.16)$$

where d_{org} is the depth of the organic layer (m) and alt is the maximum depth of thaw from the previous year (m). Thus, with a deeper organic layer and a shallower active layer, more of the roots are distributed within the organic layer (Fig. 2.21).

The potential water loss from each soil layer is then calculated as:

$$pwl_{org} = \min(pw \times r_z, 0.0) \quad (2.2.17)$$

$$pwl_{min} = \min(pw(1.0 - r_z), 0.0) \quad (2.2.18)$$

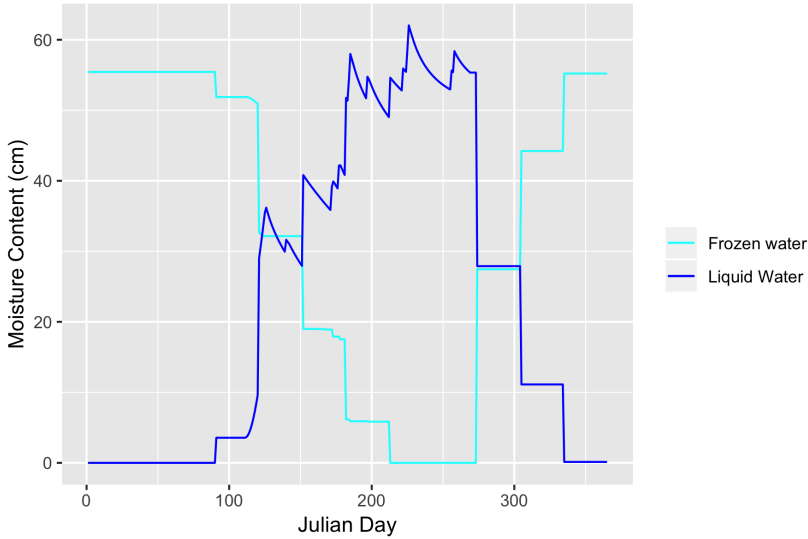


Figure 2.22: Example simulation of frozen and liquid water amounts in the soil (cm) throughout a simulation year for a site in interior Alaska.

Actual water loss from each layer (E_s , m) is calculated using an exponential equation for water retained for a given evaporative demand from Pastor and Post (1985, 1984) and Bonan (1989):

$$E_s = w_l - w_l e^{B|pwl_s|} \quad (2.2.19)$$

where pwl_s is the potential water loss from the layer (Eq. 2.2.17-2.2.18), and $B = 0.461 - 1.10559/(z_{drain}d_s)$. Finally, the amount of liquid water that freezes in each layer (w_f , m) is calculated. As in Bonan (1989), water freezes in proportion to the change depth of freezing (Section 2.2.3):

$$w_f = \left(\frac{w_l}{d_{thaw}} \right) (d_{freeze} - d'_{freeze}) \quad (2.2.20)$$

where d_{freeze} is the current day's depth of freezing (m) and d'_{freeze} is the previous day's depth of freezing (m). This amount is subtracted from the liquid water pool and added to the frozen water pool (Fig. 2.22).

Total runoff for that day (R_{tot} , m) is calculated as the sum of excess water from the soil and that due to slope runoff (Eq. 2.2.6):

$$R_{tot} = w_{exs_{min}} + R_s \quad (2.2.21)$$

Total AET (m) is calculated as evaporation from the canopy and soil layers (Fig. 2.23):

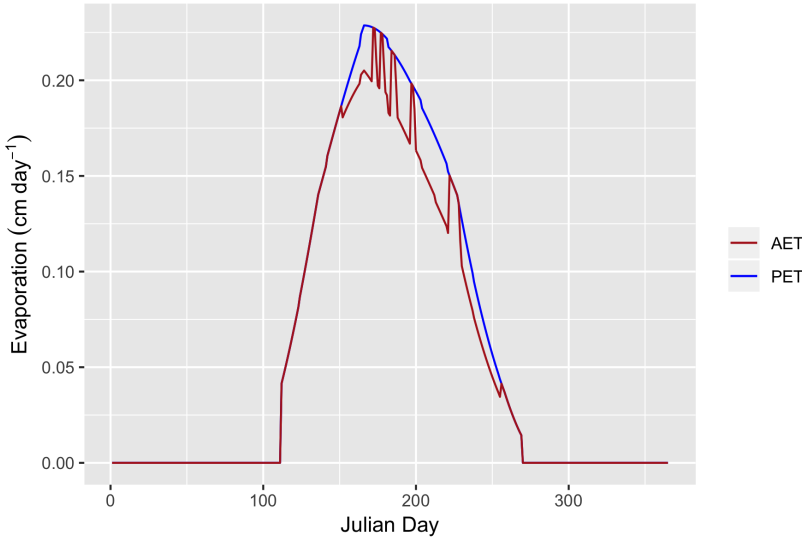


Figure 2.23: Example simulation of AET and PET for a site in interior Alaska.

$$AET = E_{can} + E_{org} + E_{min} \quad (2.2.22)$$

The daily soil water contents are used to calculate daily indices of soil dryness and saturation which are aggregated to create annual drought and saturation indices, used throughout the rest of the simulation. In this updated version, organic and mineral layer water contents are scaled by the updated wilting point and field capacity (i.e. m'_{pwp} and m'_{fc} , Eqs. 2.2.9 - 2.2.11), rather than by the static input values (see Section 2.4). Note: when the thaw depth is greater than the soil layer depth, this scaling would not impact the input wilting point and field capacity values.

2.2.2 Soil Decomposition and Soil Nutrients

In previous versions of UVAFME, any trees that died and all annual litterfall were added to site-wide pools of C and N, regardless of litter type (i.e. boles, leaves, etc.) or species (Foster et al., 2017; Yan & Shugart, 2005). These C and N amounts along with temperature and soil moisture were used to calculate soil respiration and plant-available nitrogen. This previous submodel was based on the CENTURY model's soil nutrient cycling (Parton et al., 1994) and performed well in simulating tree-soil interactions in previous applications of UVAFME (Yan & Shugart, 2005; Shuman et al., 2017; Foster et al., 2017). The updated version described below allows for finer-scale inter-

actions between climate, soils, vegetation, and disturbances through explicit tracking and decomposition of individual forest litter “cohorts”. Within the simulation, any litter from branch thinning, annual leaf-off, or tree mortality is added to a litter array along with moss litter (see Section 2.3), depending on its type and genus (for leaf litter). Litter is accumulated within the array throughout each simulation year and decomposed the following year in the updated soil decomposition subroutine (Fig. 2.24).

For bare-ground initiation runs, it is assumed that a severe fire has initiated secondary succession and thus some amount of litter and humus remain at the site. For each plot to be simulated, woody litter is initialized to a default amount of 53.5 t ha^{-1} , whereas all other litter types (i.e. leaves, twigs, roots, well-decayed wood, and moss) remain at 0.0 t ha^{-1} . Organic matter (humus) is initialized to 75 t ha^{-1} , and humus N content is initialized to 0.6 t ha^{-1} , as in Bonan (1990). Initial organic layer depth (d_{org} , m) is then calculated as (Keane et al., 2011):

$$d_{org} = (1/\text{plotsize})\left(\frac{M_{hum}}{bd_{hum}}\right) \quad (2.2.23)$$

where plotsize is the plot area (default to 500 m^2), M_{hum} is the amount of humus (kg plot^{-1}), and bd_{hum} is the bulk density for humus, set to a default value of 76.94 kg m^{-3} as in Bonan (1990).

Litter Cohorts and Characteristics

In this updated nutrient submodel, different types of litter decay at different rates according to input litter characteristics. Each year, litter from each of these different types is placed into separate cohorts which decay until they reach a critical weight at which they are transferred to either humus or well-decayed wood (Fig. 2.24). Input litter parameters (Table 2.2) are taken from Pastor and Post (1985) and Bonan (1990).

The ash parameter (α) is a correction factor to calculate ash-free weight of litter from the initial input weight. This value is multiplied by the initial cohort’s weight at the beginning of decomposition. The initial N parameter, pN_{init} is the proportion of the litter cohort’s weight that is nitrogen. This value is multiplied the the cohort’s initial ash-free weight to derive initial N weight (N_{init} , tN ha^{-1}). The immobilization parameter determines how much N (g) is immobilized per gram weight loss of the litter type, and is used to decrease the N content of decaying litter and to calculate total N immobilized during decomposition. The critical N parameter (pN_{crit}) is the critical proportion of N at which a decaying litter cohort is transferred to either well-decayed wood (for boles) or humus (all other litter types). The

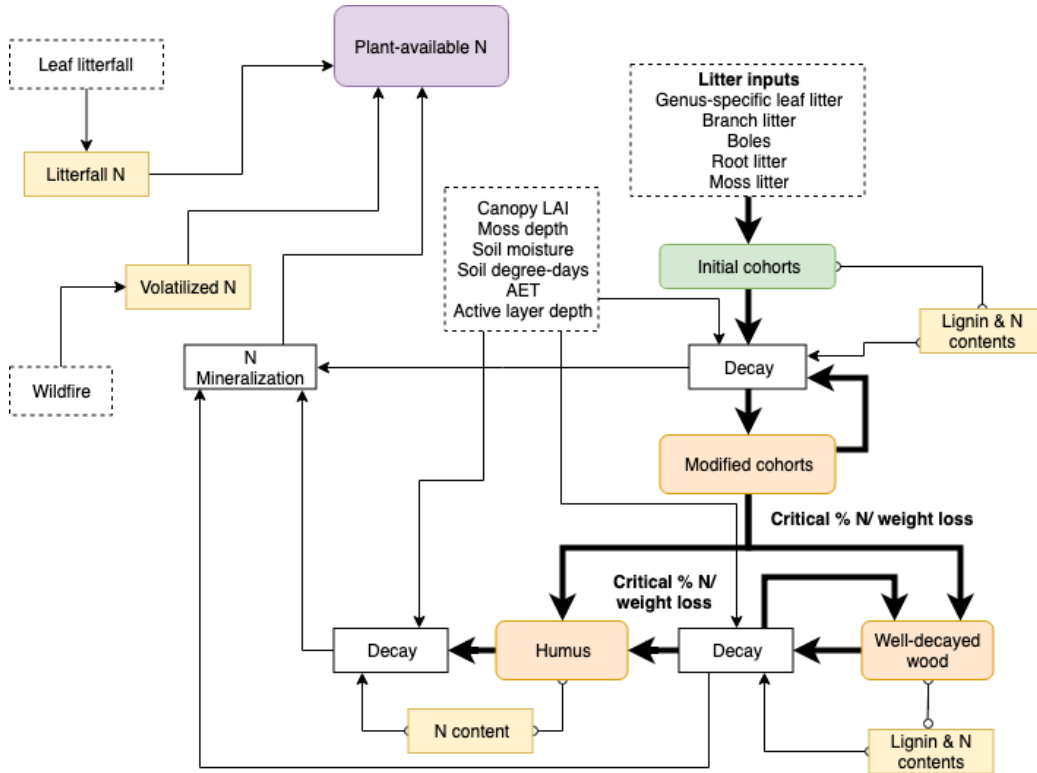


Figure 2.24: Flow diagram showing litter and decomposition dynamics simulated in UVAFME.

Table 2.2: Input litter parameters. Values taken from Pastor and Post (1985) and Bonan (1990).

Litter Type or Genus	Initial N	g Immobilized per g	Weight loss	Critical N	Initial Lignin	A	B	Ash
Cornus	0.0068	0.0251		0.0183	0.039	0.5217	0.336	0.9
Acer/Fraxinus/Tilia	0.0076	0.0315		0.0239	0.121	0.5219	0.4	0.9
Prunus	0.0109	0.0574		0.0465	0.193	0.7787	0.508	0.92
Betula	0.0106	0.0377		0.0271	0.158	0.6693	0.435	0.92
Quercus alba	0.0079	0.0256		0.0177	0.187	0.5194	0.315	0.93
Tsuga/Thuja	0.0081	0.0286		0.0205	0.206	0.6839	0.475	0.96
Populus	0.0085	0.0336		0.0251	0.214	0.7059	0.46	0.94
Fagus	0.0057	0.0477		0.042	0.241	1.1967	0.79	0.91
Quercus rubra	0.009	0.0341		0.0251	0.248	0.6105	0.359	0.95
Abies	0.0056	0.0326		0.027	0.28	0.5926	0.383	0.97
Picea	0.0063	0.022		0.0157	0.216	0.9052	0.594	0.97
Pinus	0.0046	0.0163		0.0117	0.283	0.5646	0.327	0.96
Roots	0.0096	0.0284		0.0188	0.253	0.7	0.456	0.98
Fresh wood	0.0038	0.0195		0.0157	0.173	0.4831	0.299	0.99
Twigs	0.0038	0.0195		0.0157	0.173	0.4831	0.299	0.96
Well-decayed wood	0.005	0.0364		0.0314	0.423	0.7222	0.299	0.99
Moss	0.0046	0.0215		0.0072	0	0	0	0.97

initial lignin parameter (pL_{init}) is the litter cohort's initial lignin percent. The initial lignin percent is also used to calculate the critical fraction remaining (pM_{crit}) at which a decaying litter cohort is transferred to humus or well-decayed wood:

$$pM_{crit} = 1.7039pL_{init} + 0.0955 \quad (2.2.24)$$

Finally, the parameters A and B are used to update litter lignin percent as the litter cohort decays.

Litter Decay

Cohort decay is dependent on different site conditions such as litterfall rate, light level, moisture, permafrost depth, moss cover, as well as litter characteristics. A factor to incorporate the effects of canopy gaps on litter decay (f_g) is calculated as in Pastor and Post (1985) that depends on actual litterfall relative to a closed canopy litterfall variable. Closed canopy litterfall is calculated as:

$$P_{can} = 1.54 + 0.0457(w_{fc} - w_{pwp}) \quad (2.2.25)$$

where w_{fc} and w_{pwp} are the combined field capacities and wilting points of the organic and mineral layers (cm). The total leaf litter that year (l_{leaves} , t ha $^{-1}$) along with P_{can} is used to calculate the canopy gap factor (Fig. 2.25):

$$f_g = \begin{cases} 1.0 + \left(-0.5 + 0.075(w_{fc} - w_{pwp}) \right) \left(1.0 - \frac{l_{leaves}}{P_{can}} \right), & l_{leaves} \leq P_{can}. \\ 1.0, & l_{leaves} > P_{can}. \end{cases} \quad (2.2.26)$$

As the actual litterfall decreases relative to the calculated closed canopy litterfall amount, f_g increases and thus acts to increase litter decay rate (Eq. 2.2.30).

An additional light level decay multiplier from Bonan (1990) is used that incorporates LAI:

$$f_{LAI} = \begin{cases} 1.0, & LAI \geq 2.5. \\ 1.0 + 1.5\sqrt{1.0 - LAI/2.5}, & LAI < 2.5 \end{cases} \quad (2.2.27)$$

As in the previous equation, as LAI decreases, the LAI factor increases above 1.0 (Fig. 2.26), thus increasing the decay rate (Eq. 2.2.31).

As in previous versions of UVAFME, a soil moisture factor (f_{moist}) is used to simulate the effects of soil moisture on decomposition (Foster et al., 2017). In this updated version moss depth is also incorporated into this factor.

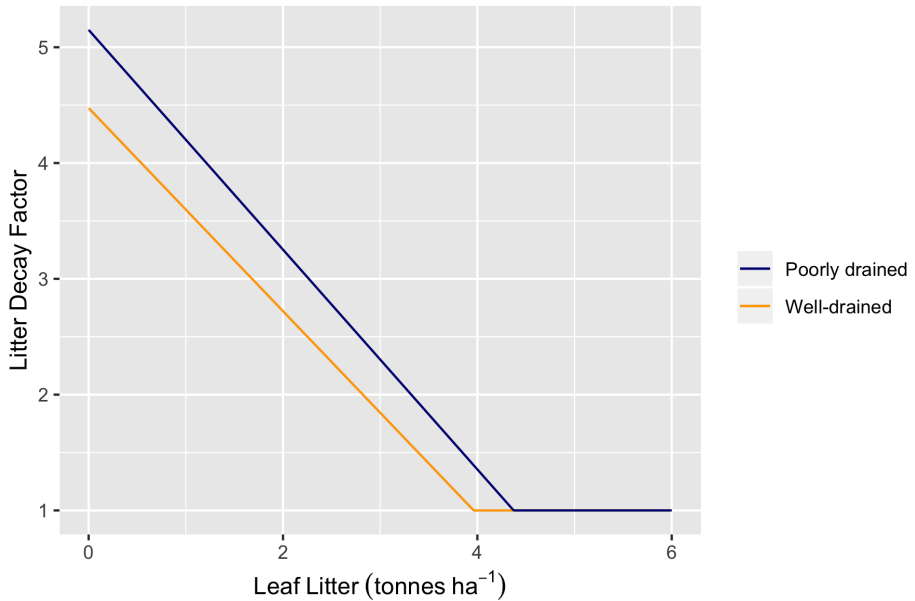


Figure 2.25: Example calculation for the litter decay factor (f_g) for a poorly drained ($w_{fc} = 68 \text{ cm}$) and well-drained ($w_{fc} = 59 \text{ cm}$) site (Eq. 2.2.26).

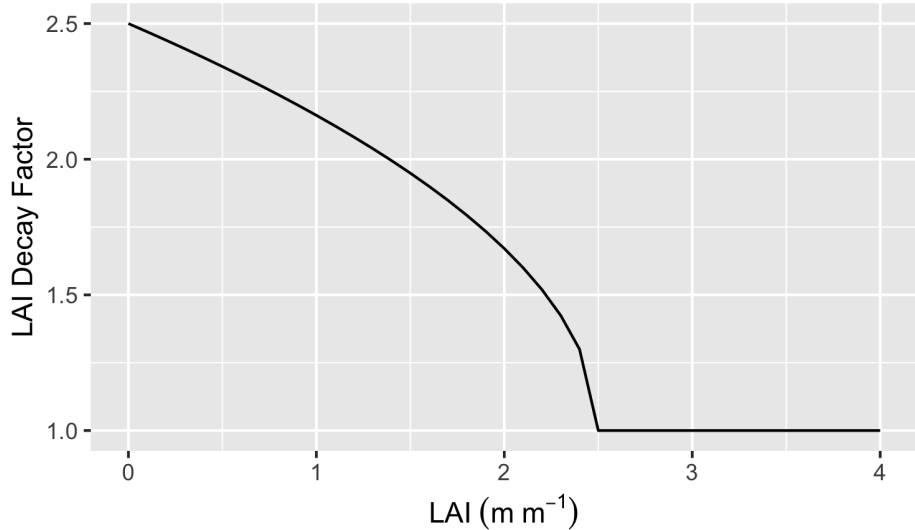


Figure 2.26: The LAI decay factor (f_{LAI}) increases with decreasing LAI; Eq. 2.2.27 (Bonan, 1990).

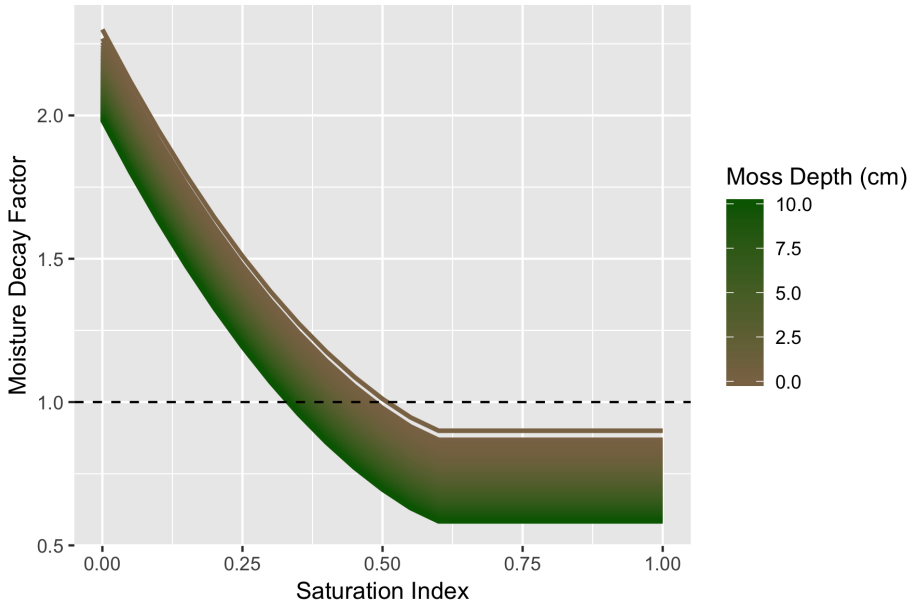


Figure 2.27: The moisture decay factor (f_{moist}) decreases with increasing saturation and increasing moss depth (Eq. 2.2.28).

$$f_{moist} = 0.5 \left[\max \left(1.6 - \sqrt{4(d_{moss} + d_{mlitter})}, 0.0 \right) + \max \left(3(1 - 1.25SI)^2, 0.2 \right) \right] \quad (2.2.28)$$

where d_{moss} and $d_{mlitter}$ are the depths of live moss and moss litter (cm), and SI is a saturation index, based on the percent of the growing season with mineral soil moisture above field capacity. As the saturation index increases and moss depth increases, f_{moist} decreases (Fig. 2.27), thus impacting litter decay.

The temperature decay factor (f_{temp}) from the previous version of UVAFME is modified for this updated version as:

$$f_{temp} = 2^{0.005(SD - 1950)} \quad (2.2.29)$$

where SD is soil degree-days (cumulative sum of temperatures above 0°C). This equation is based on a temperature coefficient Q_{10} relationship, with parameters estimated using decay rates from a litterbag study by Yarie and Van Cleve (1997) (Fig. 2.28).

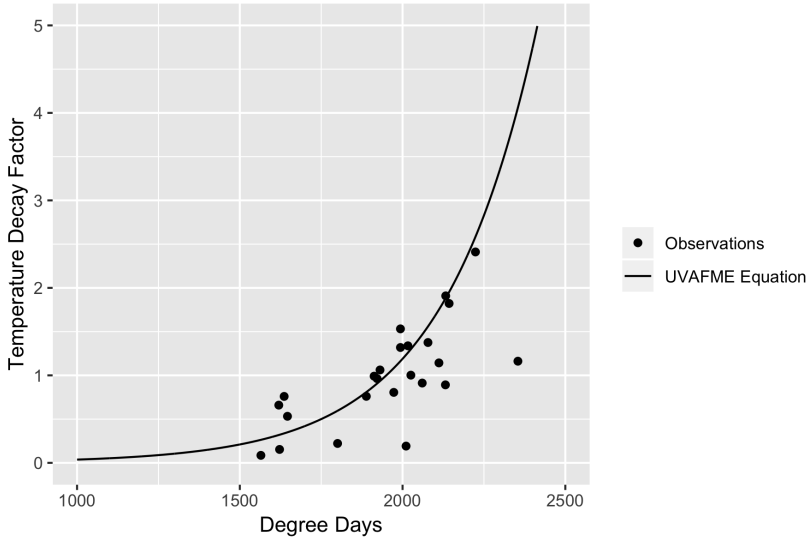


Figure 2.28: Annual decay rates normalized by average decay rate versus degree-days above 0°C along with the UVAFME temperature decay factor (Eq. 2.2.29). Observation data are from a litterbag study from 1989 to 1997 at several Bonanza Creek LTER sites (Yarie & Van Cleve, 1997) and from temperature data from the same sites and years (Van Cleve et al., 2017).

Percent weight loss (pM_{loss}) is then calculated as a function of these multipliers in addition to other site-level metrics. For this updated version a combination of two different equations for percent weight loss is used from Pastor and Post (1985) and Bonan (1990). Pastor and Post's equation uses f_g as well as site-level evapotranspiration (AET , mm), and the lignin:N ratio of the litter to calculate annual percent weight loss:

$$pM_{lossPP} = 0.01f_g \left(\left(0.9804 + 0.09352AET \right) - \left(pL : pN(-0.4956 + 0.00193AET) \right) \right) \quad (2.2.30)$$

where pL and pN are the cohort's current percent lignin and percent N. Bonan's equation uses the percent N of the litter as well as f_{LAI} and active layer depth (alt , m):

$$pM_{lossB} = f_{LAI} \left((-0.0052 + 2.08pN)e^{0.898alt} \right) \quad (2.2.31)$$

In this updated version, if the active layer depth is less than 1.5 m, the

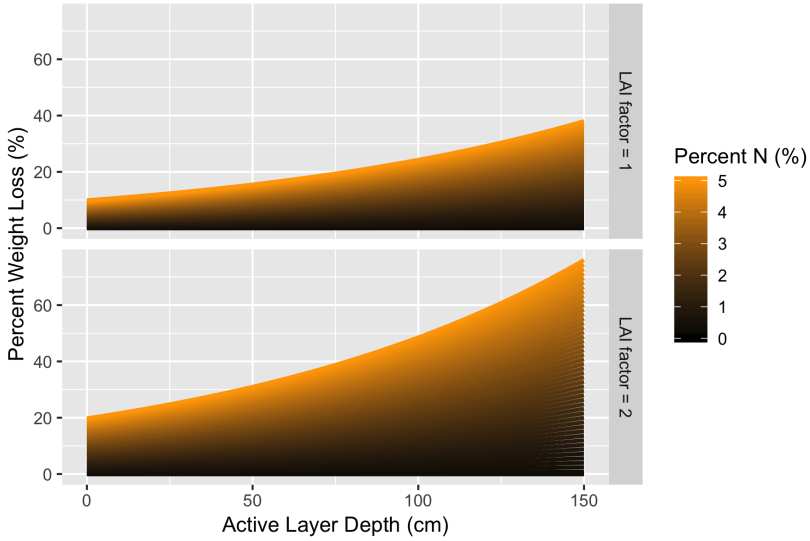


Figure 2.29: Example calculation of percent weight loss from Bonan (1990) (Eq. 2.2.31).

percent weight loss (pM_{loss}) is calculated as an average of Bonan's (Fig. 2.29) and Pastor and Post's equation (Fig. 2.30), otherwise only Pastor and Post's equation is used (note: for decay of moss litter, only Bonan's equation is used, regardless of active layer depth).

These percent weight loss calculations are then modified as: $pM_{loss} = \min(\max(pM_{loss}f_{temp}f_{moist}, 0.0), 1.0)$, and further modified as in Pastor and Post (1985) such that the weight loss of large boles is 3%, weight loss of small boles is 10%, weight loss of well-decayed wood is 5%, and weight loss of twigs is a maximum of 20%.

The actual weight loss is calculated as the percent weight loss times the current weight of the litter cohort ($M_{loss} = pM_{loss}M$), and the fraction of the original input organic matter remaining is then calculated as:

$$pM_{rem} = (M - M_{loss})/M_{init} \quad (2.2.32)$$

The new N concentration after weight loss is calculated as:

$$pN = gN - pN_{crit}pM_{rem} \quad (2.2.33)$$

where gN is an input litter parameter (Table 2.2) representing the grams of N immobilized per gram weight loss. These values are used to determine if each cohort will remain to decay further the following year or if the remaining organic matter will be transferred to humus or well-decayed wood. If the

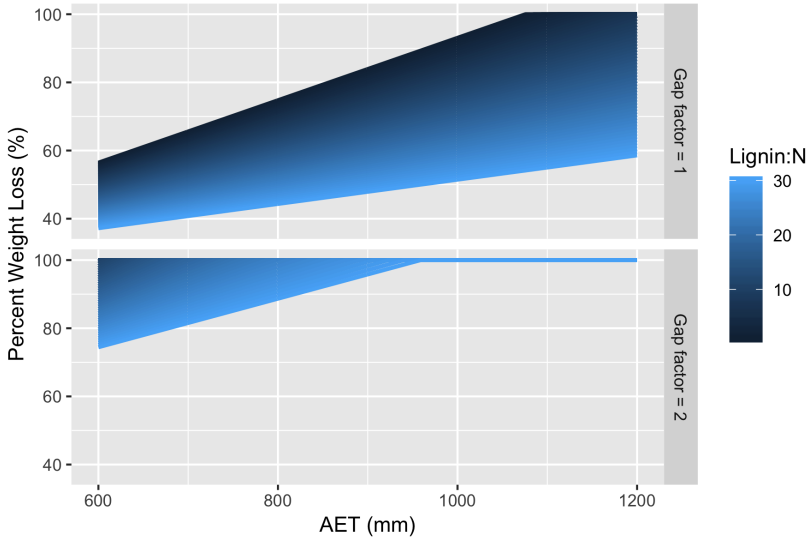


Figure 2.30: Example calculation of percent weight loss from Pastor and Post (1985) (Eq. 2.2.30).

percent remaining is less than the critical fraction remaining (pM_{crit}), then the cohort is transferred. When this occurs, the actual weight loss and N concentration are recalculated as:

$$M_{loss} = M - pM_{crit}M_{init} \quad (2.2.34)$$

and

$$pN = gN - pN_{crit}pM_{crit} \quad (2.2.35)$$

The absolute change in N content as a result of decay is calculated as the difference between the N content before this year's decay and the N content of the litter cohort as a result of this year's decay: $\delta N = M_N - pN(M - M_{loss})$. If this value is negative, then the total year's N immobilization is increased by $|\delta N|$, otherwise the total year's N mineralization is increased by δN . The final weight and N content of these cohorts are then transferred to either humus (all litter except boles) or well-decayed wood (boles). For moss litter, transferal to humus is calculated using critical weight loss rather than critical percent remaining, as in Bonan (1990). Critical weight loss is calculated as the weight loss required for the current N concentration to equal the N concentration at which moss is transferred to humus (Table 2.2):

$$M_{losscrit} = \frac{pN_{crit}M - M_N}{gN + pN_{crit}} \quad (2.2.36)$$

If the actual weight loss is greater than or equal to the critical weight loss, then the moss cohort is transferred to humus and weight loss is set equal to the critical weight loss amount. The N concentration of the moss cohort is updated to equal the critical N concentration. The N content that is transferred to the humus N pool is then calculated as $M_{loss}gN$ and the remaining moss weight is transferred to the humus pool. The immobilization/mineralization amount is updated as with the other litter cohorts.

If the percent organic matter remaining is greater than the critical percent (for all cohorts but moss), the litter cohort is not transferred and is left to decay further the following year. The current weight and N amount are updated to reflect the weight loss and the lignin concentration is updated as:

$$pL = A - B \frac{M}{M_{init}} \quad (2.2.37)$$

where A and B are lignin change parameters (Table 2.2). For moss cohorts, if the weight loss is less than the critical weight loss, the cohort is not transferred to humus and the current weight is updated with the weight loss amount. The N content and concentrations are then updated as: $M_N = M_N + M_{loss}gN$ and $pN = M_N/M$.

Humus Decomposition

Humus decomposition occurs according to the active layer depth, the N concentration of the humus layer, as well as the previous decay multipliers. When the active layer depth is below 1.5 m, the percent weight loss equation from Bonan (1990) is used, otherwise a separate equation, modified from Pastor and Post (1985) is used:

$$pM_{loss} = \begin{cases} f_{moist}f_{temp}f_{LAI}\left((-0.0052 + 2.08pN)e^{0.898alt}\right), & alt \leq 1.5 \\ 0.035f_gf_{moist}f_{temp}, & alt > 1.5 \end{cases} \quad (2.2.38)$$

The humus N mineralization is calculated as $N_{hummin} = M_N pM_{loss}$ and the organic and N contents of the humus pools are updated as $M'_N = M_N - N_{hummin}$ and $M = M(M'_N/M_N)$. Humus N mineralization and litter cohort mineralization are added together to derive total N mineralization (N_{min}) for the year. This value is used to calculate the plant-available N ($tN\text{ ha}^{-1}$) for the year:

$$N_{avail} = N_{min} - N_{immob} + N_{fire} + N_{tfall} \quad (2.2.39)$$

Table 2.3: Default bulk density values (kg m^{-3}) taken from Bonan (1990).

Litter Type	Bulk Density (kg m^{-3})
conifer leaf litter	28.6
deciduous leaf litter	100.0
twig litter	44.1
moss litter	28.6
humus	76.94

where N_{fire} is volatilized N from fires (see Section 2.5.2), and N_{tfall} is N mineralized from throughfall, set as 16% of total leaf litter N.

The organic layer depth (m) is then updated as:

$$d_{org} = (1/\text{plotsize}) \left(\left(\frac{M_{con}}{bd_{con}} \right) + \left(\frac{M_{dec}}{bd_{dec}} \right) + \left(\frac{M_{twigs}}{bd_{twigs}} \right) + \left(\frac{M_{moss}}{bd_{moss}} \right) + \left(\frac{M_{hum}}{bd_{hum}} \right) \right) \quad (2.2.40)$$

where M_{con} , M_{dec} , M_{twigs} , M_{moss} and M_{hum} are the weights of conifer leaf litter, deciduous leaf litter, twig litter, moss litter, and humus (kg plot^{-1}), and bd_{con} , bd_{dec} , bd_{twigs} , bd_{moss} , and bd_{hum} are their corresponding bulk densities (Table 2.3).

2.2.3 Permafrost

The daily depths of freeze and thaw are calculated in the permafrost subroutine using the Stefan equation as in Bonan (1989), by determining the required number of monthly cumulative degree-days to freeze or thaw each soil layer completely, and evaluating that against the actual number of available monthly degree-days for freezing/thawing (Fig. 2.31).

The required number of degree-days to thaw a layer of depth d_s (m) is:

$$DD_{req} = Q_l d_s / 24 \left(r_{above} + r_s / 2 \right) \quad (2.2.41)$$

where Q_l is the latent heat of fusion of the soil layer (kcal m^{-3}), r_{above} is the sum of the thermal resistances of the above soil and moss layers ($\text{m}^2 \text{ }^\circ\text{C hr kcal}^{-1}$), and r_s is the thermal resistance of the current soil layer (Jumikis, 1966; Bonan, 1989). The latent heat of fusion is calculated as:

$$Q_l = (80gw)bd_s \quad (2.2.42)$$

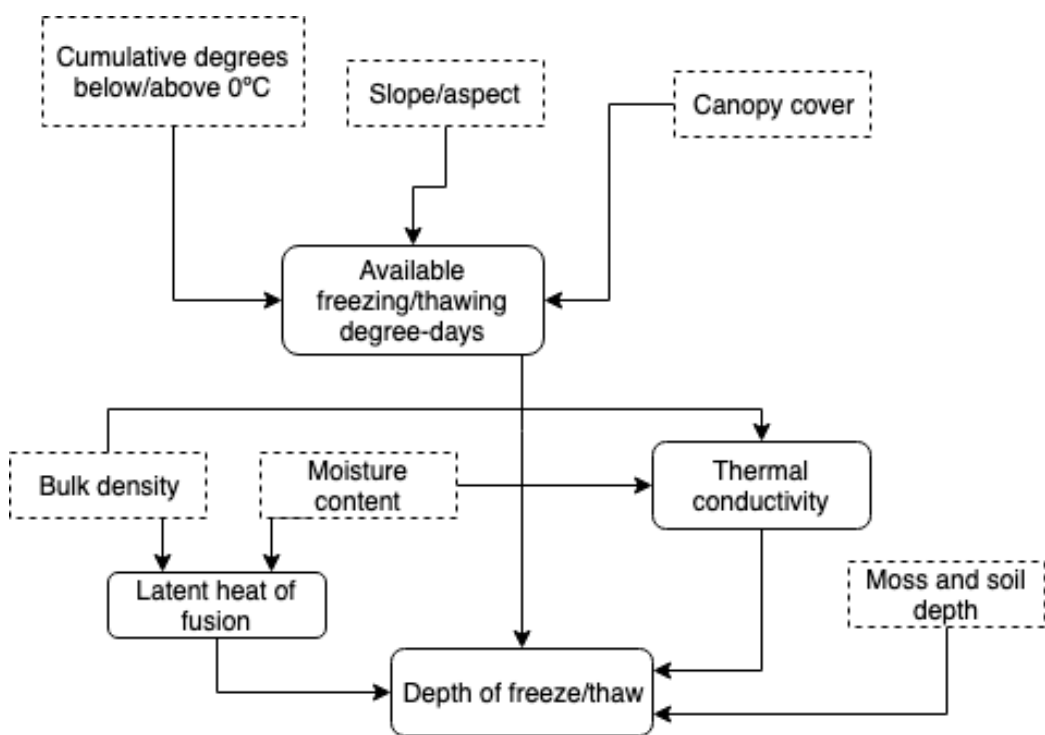


Figure 2.31: Flow diagram showing permafrost dynamics simulated in UVAFME.

where gw is soil layer's gravimetric water content ($gw = \frac{1000m_w}{bd_s}$, where m_w is the volumetric moisture content), and bd_s is the bulk density of the soil layer (kg m^{-3}) (see Section 2.2.1). The thermal resistance of the soil layer is calculated as $r_s = d_s/k_s$ where k_s is the soil layer's thermal conductivity ($\text{kcal m}^{-1} \text{ hr}^{-1} \text{ }^\circ\text{C}^{-1}$).

The available degree-days for thawing and freezing (i.e. cumulative monthly degrees above/below 0°C) are adjusted to account for vegetation cover and light on the forest floor, as well as slope and aspect. Using the canopy openness on the plot, calculated as: $al = e^{-0.25LAI}$, separate correction factors are determined for freezing (c_f) and thawing (c_t) degree-days. For $al > 0.75$, $c_t = 0.92$ and $c_f = 0.36$. For $0.50 < al \leq 0.75$, $c_t = 0.77$ and $c_f = 0.37$. For $al \leq 0.50$, $c_t = 0.62$ and $c_f = 0.38$. The topographic correction factor is calculated as: $c_s = R/R_H$ where R/R_H is the ratio of actual surface radiation to horizontal surface radiation (see Section 2.1.2). The available freezing (DD_f) and thawing (DD_t) degree-days are then modified as:

$$DD_f = DD_f c_f (2 - c_s) \quad (2.2.43)$$

and

$$DD_t = DD_t c_t c_s \quad (2.2.44)$$

Thus, available freezing degree-days decrease with increasing light (i.e. decreasing vegetation cover). The topographic factor acts to decrease available freezing degree-days with sites that have higher actual surface radiation than horizontal surface radiation (i.e. south-facing slopes), and increase freezing degree-days for sites with lower actual surface radiation than horizontal surface radiation (i.e. north-facing slopes). The available thawing degree-days decrease less with increasing available light. The topographic factor acts to increase available thawing degree-days with south-facing slopes, and decreases them for north-facing slopes.

The thermal conductivities of the moss-organic layer and the mineral layer are calculated using the moisture contents, bulk densities, wilting points, and field capacities of the soil layers. As in Bonan (1989), the frozen (k_f) and unfrozen (k_u) thermal conductivities of the moss-organic layer are calculated as:

$$k_u = \frac{(0.5(m_{pwp} - m_w) + 0.08(m_w - m_{fc}))}{m_{pwp} - m_{fc}} \quad (2.2.45)$$

and

$$k_f = \frac{(2.0k_u(m_{pwp} - m_w) + k_u(m_w - m_{fc}))}{m_{pwp} - m_{fc}} \quad (2.2.46)$$

where m_{fc} and m_{pwp} are the field capacity and wilting points (volumetric) of the layer. Also as in Bonan (1989), the thermal conductivities for the mineral soil layer (here in Btu in ft^{-2}) are calculated using equations from Lunardini (1981), using separate equations for fine-textured and granular soils:

Fine-textured:

$$k_u = (0.9 \log_{10}(100gw) - 0.2) \times 10^{0.01bde_s} \quad (2.2.47)$$

$$k_f = 0.01 \times 10^{0.022bde_s} + 0.085(100gw) \times 10^{0.008bde_s} \quad (2.2.48)$$

Granular:

$$k_u = (0.7 \log_{10}(100gw) + 0.4) \times 10^{0.01bde_s} \quad (2.2.49)$$

$$k_f = 0.076 \times 10^{0.013bde_s} + 0.032(100gw) \times 10^{0.0146bde_s} \quad (2.2.50)$$

where bde_s is the bulk density of the soil in lb ft^{-3} . Once the available degree-days and required degree-days for each layer are calculated, the two values are compared. If the available degree-days is greater than or equal to the required degree-days, the depth of freeze/thaw of that layer is set to the entire layer's depth, and the available degree-days is decremented by that layer's required degree-days. The model then moves to the lower layer and compares the available degree-days again to the required degree-days.

If the required degree-days is greater than the available degree-days, the available degree-days is set to 0.0, and the depth of freeze/thaw for that layer is calculated using a quadratic formulation:

$$x = \frac{-b + \sqrt{b^2 - 4ac}}{2a} \quad (2.2.51)$$

where $a = \frac{0.5Q_l}{k_{f,t}}$, $b = Q_l r_{above}$, and $c = -24DD_{f,t}$. Finally, the depths of freeze/thaw for each layer are summed to derive the total depth that day (d_{melt} and d_{freeze}). These values are used to update the seasonal maximum depths of freeze (z_{freeze}) and thaw (alt), and also impact soil water dynamics, decomposition, and tree growth (see Sections 2.2.1, 2.2.2, and 2.4).

2.3 Moss

A moss growth and decay subroutine was added to this updated version of UVAFME to calculate the annual growth and decay of moss. As in Bonan and Korzukhin (1989), moss growth is modeled as the difference between carbon assimilation and decay/respiration. Due to bryophyte's simple allocation scheme, the relationship between moss photosynthesis and growth/productivity is fairly tight compared to vascular plants (Oechel & Van Cleve, 1986), and thus this relatively simple model of moss growth is appropriate. Carbon assimilation is assumed to be proportional to maximum moss biomass reported for interior Alaska (0.2 kg m^{-2} ; Van Cleve and Viereck (1981)), and is modified based on plot conditions such as light level, soil moisture, and tree litterfall.

2.3.1 Moss Growth Factors

Light Extinction and Forest Floor Light Conditions

As in Bonan and Korzukhin (1989), a light extinction factor is derived to simulate the effect of light availability on moss photosynthesis. Here, light availability is calculated as:

$$L_{avail} = e^{-\gamma S_\mu M_{biom}/2} \quad (2.3.1)$$

where M_{biom} is current moss biomass (kg m^{-2}), S_μ is a specific leaf area parameter, set to 1.7, and $\gamma = 3.5$. Parameter values are taken from Bonan and Korzukhin, where they were derived from data on moss growth from Van Cleve et al. (1983) and Larcher (1980). The effect of this light availability on assimilation is then calculated as:

$$f_{ext} = \frac{a_1(L_{avail} - a_3)}{1.0 + a_2 L_{avail}} \quad (2.3.2)$$

where a_1 and a_2 are light curve parameters, set to 3.41 and 2.14 from Bonan and Korzukhin (1989), and a_3 is a light compensation point for factor, set to 0.08 from Bonan and Korzukhin (1989). A second light factor is calculated to simulate the effect of the tree canopy on moss growth (Bonan & Korzukhin, 1989). Increases in canopy openness leads to desiccation of moss and thus this factor decreases with increasing canopy openness above 50%:

$$f_{can} = \begin{cases} 1.25 - al^2, & al > 0.5. \\ 1.0, & al \leq 0.5. \end{cases} \quad (2.3.3)$$

where $al = e^{-0.25LAI}$. To simulate the effect of the tree canopy lowering light availability for moss photosynthesis, another light factor is calculated that increases with increasing canopy openness below 50%:

$$f_{shade} = \begin{cases} b_1 + b_2\sqrt{al}, & al \leq 0.5. \\ 1.0, & al > 0.5. \end{cases} \quad (2.3.4)$$

where b_1 and b_2 are parameters, set to 0.8 and 0.8 in this updated version based on moss growth data from Jean et al. (2017). Together, these factors create a parabolic function with moss biomass increasing to a point (50% cover) and then subsequently decreasing.

Deciduous Litter and Soil Moisture

A deciduous litter factor (f_{decid}) is calculated to incorporate deciduous litter's inhibition of moss growth and establishment. Using data from (Jean et al., 2017), this factor is calculated as:

$$f_{decid} = \begin{cases} 1.0 - 75M_{decid}, & M_{decid} > 0.0. \\ 1.0, & M_{decid} = 0.0. \end{cases} \quad (2.3.5)$$

where M_{decid} is the mass of deciduous leaf litter on the plot ($t \text{ ha}^{-1}$). As in Bonan and Korzukhin (1989), a soil moisture growth factor (f_{moist}) is used to simulate desiccation of the moss layer at low moisture levels. If the drought index (DI , see Section 2.4) for the year is below 0.10 moss is not allowed to grow. Otherwise, moss is allowed to grow normally:

$$f_{moist} = \begin{cases} 1.0, & DI \leq 0.10. \\ 0.0, & DI > 0.10. \end{cases} \quad (2.3.6)$$

2.3.2 Moss Growth and Decay

The assimilation rate (A_r , kg kg^{-1}) is calculated as a function of the maximum moss growth and the previous growth factors:

$$A_r = \mu f_{shade} f_{ext} f_{moist} f_{can} f_{decid} \quad (2.3.7)$$

where μ is maximum moss productivity (kg m^{-1}). Moss respiration (R), is then calculated as a function of moss biomass, deciduous litter, and soil moisture:

$$R = S_\mu M_{biom}(q + b_1) + s f_{moist} f_{decid} \quad (2.3.8)$$

where q , b_1 , and s are parameters taken from Bonan and Korzukhin (1989), set to 0.12, 0.136, and 0.001. Moss growth for the year is then calculated as the difference between assimilation and respiration:

$$P = S_\mu M_{biom} A_r - R \quad (2.3.9)$$

This value can be positive (for moss growth) or negative (if respiration is greater than assimilation). The growth amount is then added to the current year's biomass. If this value is positive (i.e. moss growth occurred or mortality did not exceed the current biomass), moss biomass is updated to reflect the growth ($M'_{biom} = M_{biom} + P$). If the value is negative, P is set to $-M_{biom}$ and M'_{biom} is then set to 0.0.

Moss litter (M_{litter} , kg m⁻²) is calculated as a function of the current year's moss biomass, deciduous litter, soil moisture and growth that year.

$$M_{litter} = S_\mu M_{biom} (A_r - q) + s f_{moist} f_{decid} - P \quad (2.3.10)$$

This litter amount is added to the set of litter cohorts for decomposition (see Section 2.2.2). The depth of live moss (m) is calculated as $\frac{M'_{biom}}{bd_{moss} plotsize}$, where *plotsize* is the area of the plot (default to 500 m² in UVAFME), and *bd_{moss}* is live moss bulk density, set to a default value of 5.2 kg m⁻³. This moss depth acts to influence permafrost dynamics (see Section 2.2.3 as well as tree regeneration (Section 2.6).

2.4 Tree Growth

Tree growth in UVAFME is modeled annually as diameter increment growth, based on first simulating optimal diameter increment growth from Botkin, Janak, and Wallis (1972) and Leemans and Prentice (1989) and subsequently modifying that optimal growth based on environmental conditions and species- and tree size-specific tolerances (Yan & Shugart, 2005). Each year the updated diameter is used to calculate other tree characteristics such as height, leaf area, and biomass using allometric equations.

2.4.1 Tree Allometry

Optimal diameter growth of a tree (δDBH_{opt} , cm) is calculated as (Botkin et al., 1972):

$$\delta DBH_{opt} = gDBH \frac{1.0 - \frac{DBH \times H}{DBH_{max}/H_{max}}}{2.0H + sDBH e^{\frac{-sDBH}{H_{max}-1.3}}} \quad (2.4.1)$$

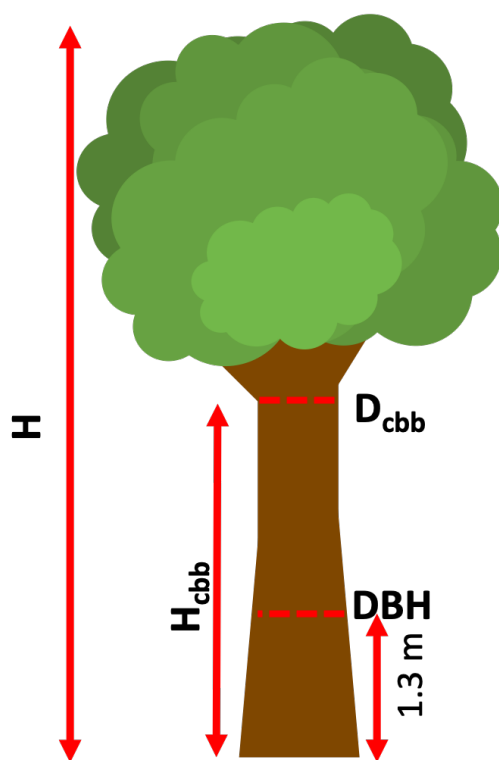


Figure 2.32: Tree measurements used in tree allometric equations.

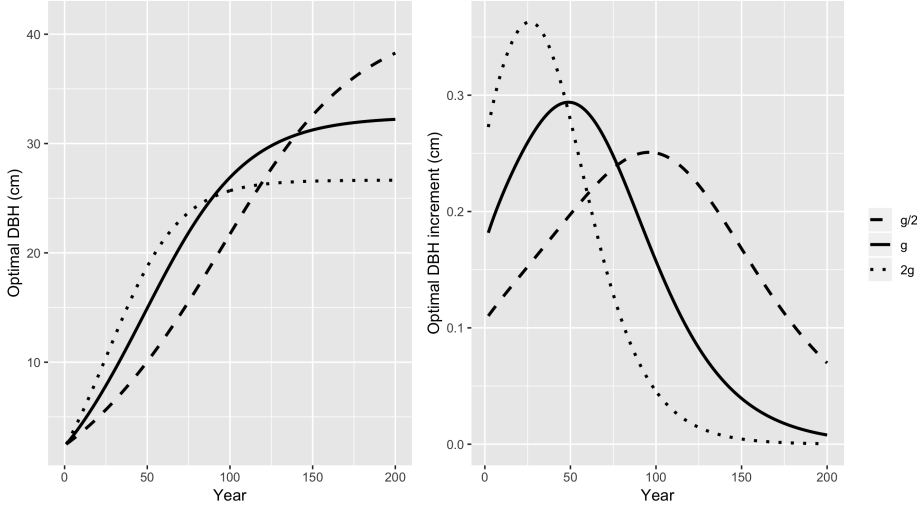


Figure 2.33: Example calculation of optimal diameter over time with changing growth parameter g ($s = 2.02$; $g = 0.748$; $H_{max} = 22$ m; $DBH_{max} = 23$ cm; $AGE_{max} = 140$ years) (Eq. 2.4.1).

where H is the current tree height (m), DBH is the current diameter at breast height (cm), H_{max} is the species' average maximum height (m), DBH_{max} is the species' average maximum DBH (cm), and s and g are species-specific growth parameters. As in Botkin et al. (1972), g is related to the initial rapid rise in diameter of an individual and higher values of g result in faster growth initially (Fig. 2.33). The parameter s is the initial slope of the optimal height-diameter relationship of a tree species.

Tree height is calculated based on an equation from the FORSKA model (Leemans & Prentice, 1989).

$$H = 1.3 + (H_{max} - 1.3)(1.0 - e^{-\frac{sDBH}{H_{max}-1.3}}) \quad (2.4.2)$$

Here, higher values of the input parameter s result in faster height growth (Fig. 2.34).

Leaf area (LA , m^2) is calculated as a function of the diameter at clear branch bole height, based on the Shinozaki pipe model (Shinozaki et al., 1964; Yan & Shugart, 2005):

$$LA = D_{cbb}^2 D_L \quad (2.4.3)$$

where D_{cbb} is the diameter at clear branch bole height (cm) (Fig. 2.32), and D_L is a species input parameter, which ranges from 0.225 to 0.255 depending on species-specific shade tolerance. Diameter at clear branch bole

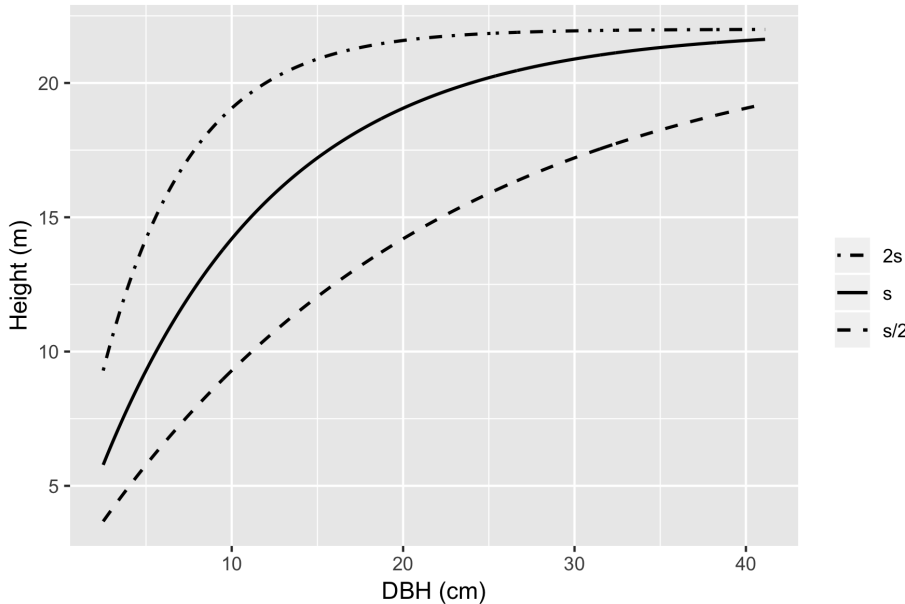


Figure 2.34: Example calculation of height vs. DBH with changing values of s ($s = 2.02$; $g = 0.748$; $H_{max} = 22$ m; $DBH_{max} = 23$ cm; $AGE_{max} = 140$ years) (Eq. 2.4.2).

height is calculated assuming a conical bole shape (Yan & Shugart, 2005):

$$D_{cbb} = \begin{cases} DBH, & H \leq 1.3 \\ DBH \left(\frac{H - H_{cbb}}{H - 1.3} \right), & H > 1.3 \end{cases} \quad (2.4.4)$$

where H_{cbb} is clear branch bole height (m). In UVAFME, H_{cbb} is not calculated allometrically but set to an initial value (1.0 m) when a tree is first initialized (Section 2.6). It can then increase annually (or not) via lower branch thinning (Section 2.4.3) (Yan & Shugart, 2005). Wood volume (i.e. biomass) is calculated assuming the bole shape is a simple cone. This volume is then multiplied by the bulk density of the wood (a species-specific input parameter) and divided by 2 to derive biomass in tonnes of C.

$$B_{bole} = 0.9bd \left(\frac{1E-4\pi 0.25DBH^2H}{3} \right)^{0.5} \quad (2.4.5)$$

where bd is the wood bulk density of the species (tonnes m^{-3}). Biomass of branches and the bole above the diameter at clear branch bole height is calculated also assuming the volume is a cone and applying similar scaling factors to derive tonnes C:

$$B_{twigs} = bd \left(\frac{1E-4\pi 0.25 D_{cbb}^2 (H - H_{cbb})}{3} \right) 0.5 \quad (2.4.6)$$

The lateral root volume is assumed to be half of the branch volume, and the root ball volume is calculated by assuming a cone at DBH height downwards to the root depth (d_{roots} , m):

$$B_{roots} = 0.5B_{twigs} + B_{bole} \frac{d_{roots}}{H} \quad (2.4.7)$$

The final total tree woody biomass is derived by summing all parts of the tree ($B_{tree} = B_{bole} + B_{twigs} + B_{roots}$). Leaf biomass is derived using leaf area:

$$B_{leaf} = 2.0LMA \times LA \quad (2.4.8)$$

where LMA is leaf mass per area (tonnes C m⁻²), set to 5×10^{-5} for evergreen and 3.16×10^{-5} for deciduous species.

2.4.2 Growth Modifiers

Annual tree growth is simulated using the above allometric equations for growth, modified by the current environmental conditions on the plot as well as species- and tree size-specific tolerances. Optimal diameter increment growth (via equation 2.4.1) is decreased based on soil moisture, temperature, light conditions, nutrient availability, and permafrost conditions (if present). For each of these potential stressors, growth factors are calculated (0 to 1) on a species- and tree-level basis and used to decrease the optimal growth of each tree to derive actual diameter increment growth. For a given plot on a given year, the environmental conditions determine how well each individual tree grows that year. Thus, trees of differing species and sizes will respond differently each year and can compete with one another for resources.

Temperature

Tree growth response to temperature is modeled using response to growing degree-days (i.e. cumulative sum of daily temperatures above 5°C). As in Foster et al. (2017) and Shuman et al. (2017), temperature response is modeled as an asymptotic increase with increasing growing degree-days, depending on species-specific growing degree-day tolerances. This asymptotic growth response does not penalize species' growth at or above its optimum growing degree-days, but does restrict growth below this value, with no growth occurring below a species' minimum growing degree-days.

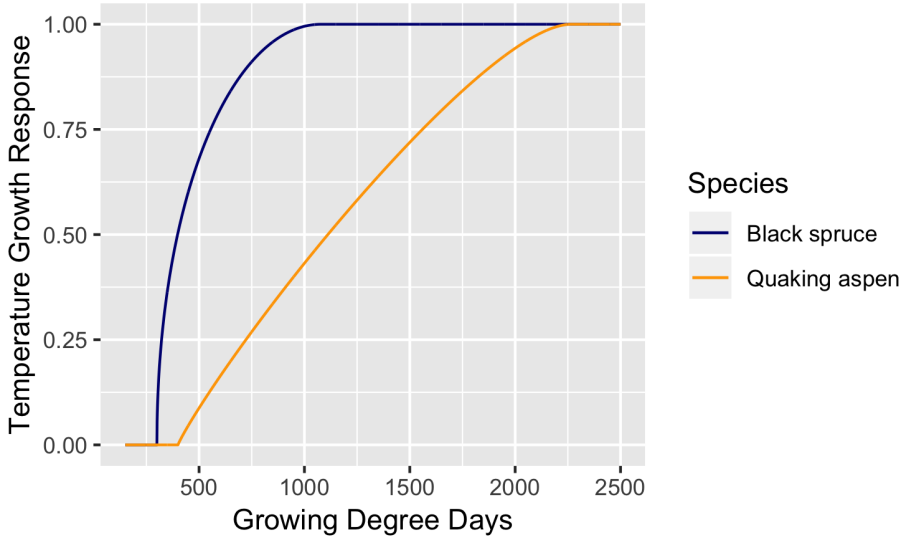


Figure 2.35: Example species growth response to growing degree-days. Black spruce: $GDD_{min} = 300$, $GDD_{opt} = 1079$, $GDD_{max} = 1911$. Aspen: $GDD_{min} = 400$, $GDD_{opt} = 2268$, $GDD_{max} = 2461$. (Eq. 2.4.9).

$$f_{gdd} = \begin{cases} 0.0, & GDD \leq GDD_{min} \\ \frac{GDD - GDD_{min}}{GDD_{opt} - GDD_{min}}^a \frac{GDD_{max} - GDD}{GDD_{max} - GDD_{opt}}^b, & GDD_{min} < GDD < GDD_{opt} \\ 1.0, & GDD \geq GDD_{opt} \end{cases} \quad (2.4.9)$$

where $a = \frac{GDD_{opt} - GDD_{min}}{GDD_{max} - GDD_{min}}$, $b = \frac{GDD_{max} - GDD_{opt}}{GDD_{max} - GDD_{min}}$, and GDD_{min} , GDD_{opt} , and GDD_{max} , are the minimum, optimum, and maximum growing degree-days for a species.

Soil Moisture

The growth factor for moisture availability is calculated based on soil moisture conditions throughout the year as well as the ratio of precipitation to PET and AET to PET. Using the daily simulation of soil moisture (section 2.2.1), indices are derived that relate a single day's soil moisture to the field capacity and wilting point of the soil. Two drought indices (ranging from 0 to 1) are utilized: DI_u and DI_b . DI_u represents the proportion of the growing season where $SW_{FC} < 0.75$, where $SW_{FC} = \frac{w_{l_{min}}}{m_{fc_{min}}}$. Here, $w_{l_{min}}$ is mineral layer liquid water content (m) and $m_{fc_{min}}$ is mineral layer field capacity (m). DI_b is represents the percent of the growing season where $SW_{WP} < 1.2$,

where $SW_{WP} = \frac{w_{l_{min}}}{m_{pwp_{min}}}$. Here $m_{pwp_{min}}$ is mineral layer wilting point (m). The growing season is defined as the part of the year where the average daily temperature is above 5°C.

DI_u is further modified as the average of DI_u and DI_{clim} , where

$$DI_{clim} = 1.0 - \max \left(\min \left(\frac{P}{PET}, 1.0 \right), \min \left(\frac{AET}{PET}, 1.0 \right) \right) \quad (2.4.10)$$

These drought indices are used to calculate an annual drought growth factor (ranging from 0 to 1, with 0 indicating soil moisture as completely limiting to growth, and 1 indicating no effect of soil moisture on growth) based on species-specific drought tolerance.

$$f_{drought} = \sqrt{\frac{\max(k_{dry} - DI, 0.0)}{k_{dry}}} \quad (2.4.11)$$

where k_{dry} ranges from 0.50 to 0.01 depending on species drought tolerance. Input species-level drought tolerance ranges from 1 to 6, with 1 being the most tolerant, and 6 being the least tolerant. For species with a tolerance level of 1 (i.e. very tolerant), $DI = DI_b$, whereas for all other species $DI = DI_u$. For very tolerant species, $f_{drought}$ is further modified as the maximum (i.e. least limiting) of $b(f_{drought})$ and $f_{drought}$ calculated as above but using $DI = DI_u$, where $b = 0.33$ for evergreen species and $b = 0.2$ for deciduous species. This allows for the most tolerant species to have an extra advantage with regards to soil moisture availability (Fig. 2.36).

Light and Shading

Tree growth response to shading is modeled using available light, calculated according to the vertical distribution of leaf area (Eq. 2.4.3) on the plot. The canopy subroutine is used to calculate this vertical distribution of leaf area. This subroutine uses the leaf area from each tree on each plot to calculate an overall plot-level cumulative leaf area, distributed vertically depending on the heights of the trees on the plot (Fig. 2.4.3).

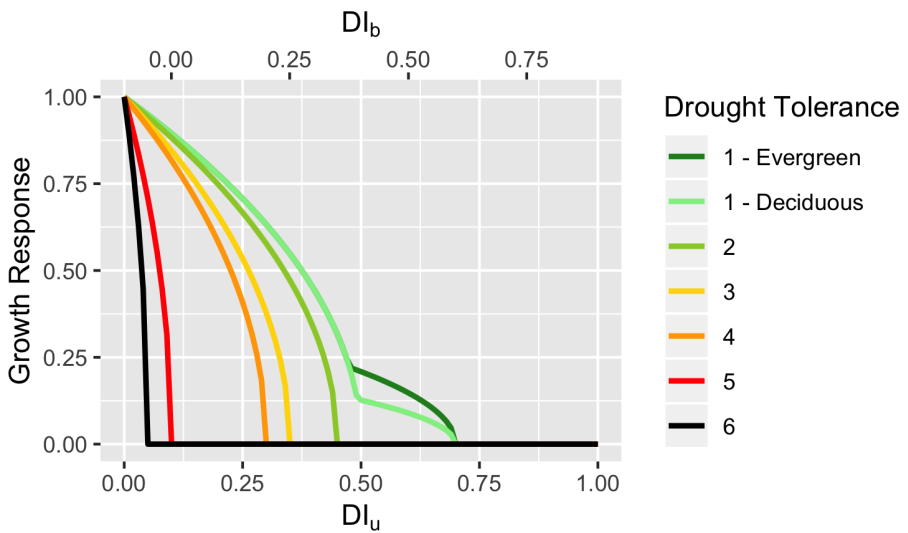


Figure 2.36: Species growth response to drought indices. DI_b is used for species with high tolerance (1). DI_u is used for all other species (Eq. 2.4.11).

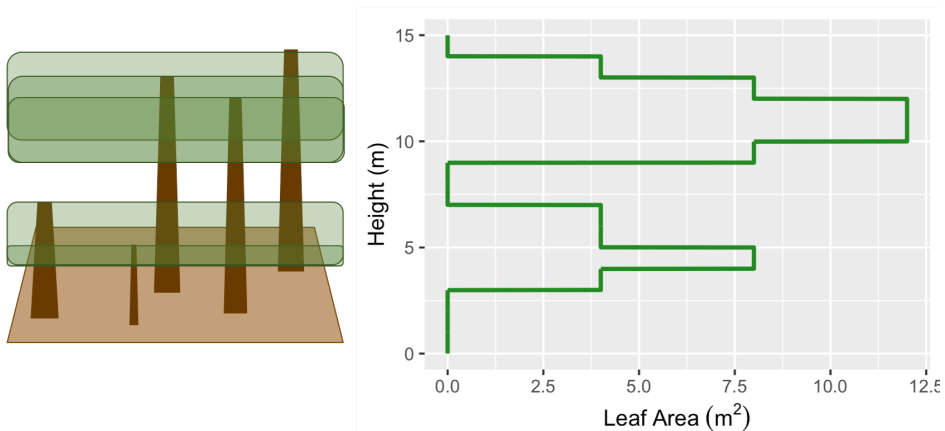


Figure 2.37: Example of vertically distributed leaf area of a plot in UVAFME. Tree canopies are assumed to be horizontally homogenous within a plot.

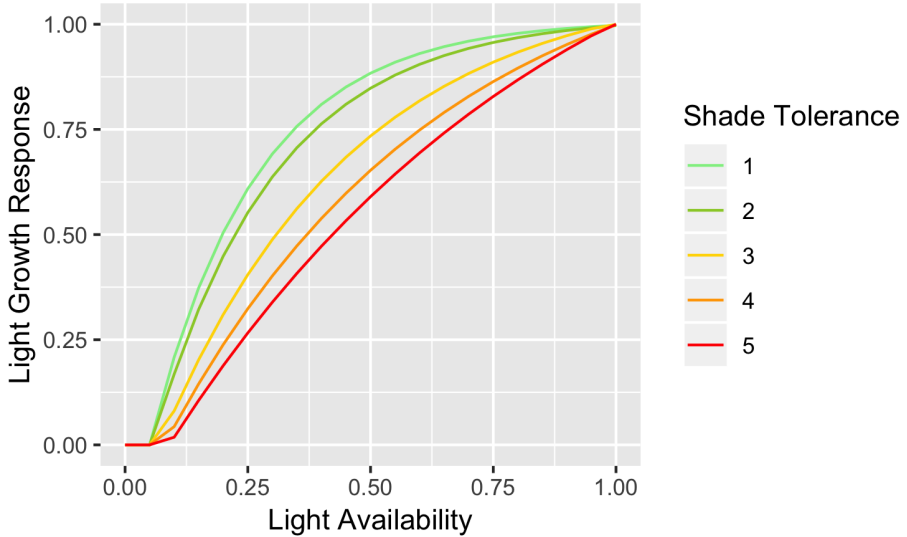


Figure 2.38: Species growth response to light availability (Eq. 2.4.13). A shade tolerance of 1 corresponds to very shade tolerant, a shade tolerance of 5 corresponds to very intolerant.

This height-structured leaf area is then used to determine light extinction through each 1-meter layer in the canopy. Deciduous leaf area experienced by evergreen species is reduced by 80% to account for the part of the year without deciduous leaf cover. This reduced leaf area results in a higher light environment for evergreen species relative to deciduous species. Light availability in the i th layer is calculated via the Beer-Lambert law:

$$L_i = e^{-cLAI_{i+1}} \quad (2.4.12)$$

where c is an extinction coefficient, set to 0.40, and LAI_{i+1} is the cumulative leaf area index (i.e. cumulative leaf area divided by plotsize, m m^{-1}) of the layer above the i th layer.

The tree growth response to light availability is calculated as:

$$f_{light} = k_{l1}(1.0 - e^{-k_{l2}(L_h - k_{l3})}) \quad (2.4.13)$$

where k_{l1} , k_{l2} , and k_{l3} depend on species-specific shade tolerance (1 through 5, 5 being least tolerant), and L_h is the light availability at the tree's height (Fig. 2.38).

Nitrogen Availability

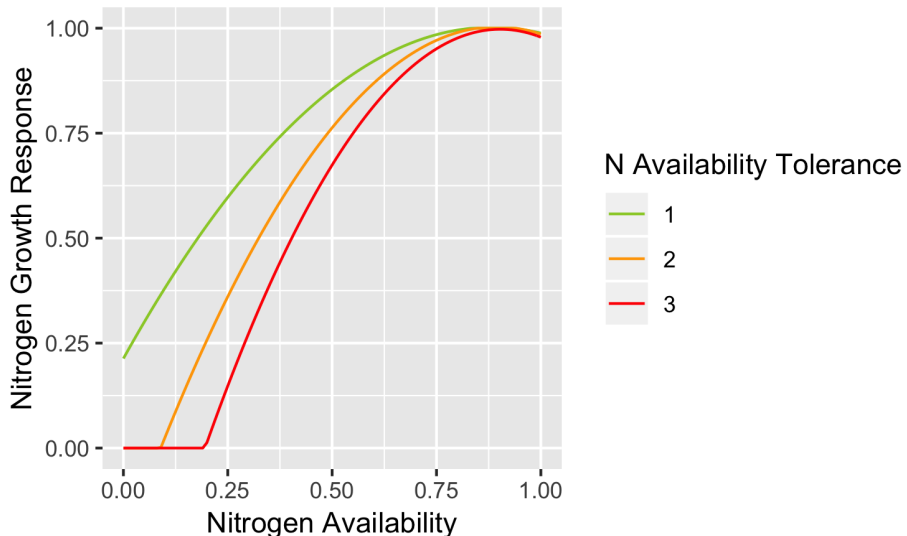


Figure 2.39: Species growth response to N availability (Eq. 2.4.14). A nitrogen tolerance of 1 corresponds to very tolerant, a nitrogen tolerance of 3 corresponds to very intolerant.

Growth response to nitrogen availability is modeled in response to a relative N availability variable, calculated using the ratio of available N to required N. Available N is calculated in the soil decomposition subroutine (Section 2.2.2). Required N is calculated by determining the actual diameter increment growth using all growth modifiers except N availability and then calculating the amount of N required for that potential growth (see Section 2.4.3).

The tree growth response to this availability ratio is:

$$f_N = k_{N1} + k_{N2}N_r + k_{N3}N_r^2 \quad (2.4.14)$$

where k_{N1} , k_{N2} , and k_{N3} depend on species-specific nutrient availability tolerance (1 to 3, 3 being least tolerant), and N_r is the ratio of available N to required N (Fig 2.39).

Permafrost

If permafrost is present, optimal tree growth is also decreased based on active layer depth (see Section 2.2.3) and species-specific permafrost tolerance

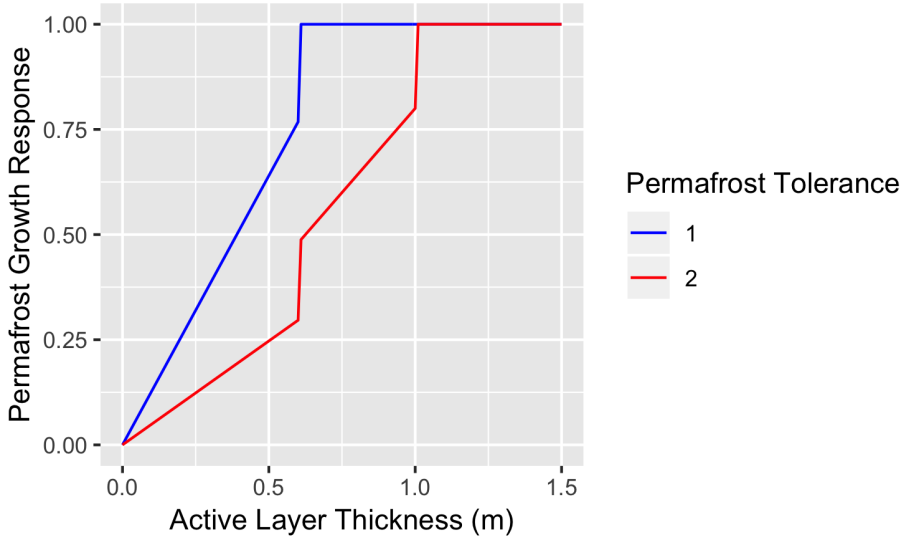


Figure 2.40: Species growth response to active layer depth (Eq. 2.4.15) for tolerant (1) and intolerant (2) species.

(tol_{perm} , 1: tolerant, 2: intolerant). Tree growth response to permafrost presence is based on equations from Bonan (1989) (Fig. 2.40):

$$f_{perm} = \begin{cases} 1.28alt, & alt \leq 0.6 \text{ and } tol_{perm} = 1 \\ 0.494alt, & alt \leq 0.6 \text{ and } tol_{perm} = 2 \\ 1.0, & 0.6 < alt \leq 1.0 \text{ and } tol_{perm} = 1 \\ 0.8alt, & 0.6 < alt \leq 1.0 \text{ and } tol_{perm} = 2 \\ 1.0, & alt > 1.0 \end{cases} \quad (2.4.15)$$

where alt is active layer thickness (m).

2.4.3 Annual Growth

Annual tree growth is modeled based on first calculating optimal diameter increment growth (Eq. 2.4.1), and then decreasing that growth based on soil moisture, light availability, temperature, and permafrost (if present). This version of UVAFME uses Liebig's Law of the Minimum (as in Pastor and Post (1985)) to decrease growth, assuming that trees are only growth limited by their most limiting stressor (apart from permafrost, which is used as a multiplicative factor):

$$\delta DBH'_{actual} = \delta DBH_{opt} f_{perm} \times \min(f_{gdd}, f_{drought}, f_{light}) \quad (2.4.16)$$

Here the effect of N availability on tree growth is not yet incorporated into the intermediate value of DBH growth. This intermediate $\delta DBH'_{actual}$ is used to calculate intermediate values of height (H' , Eq. 2.4.2), diameter at clear branch bole height (D'_{cbb} , Eq. 2.4.4), leaf biomass (B'_{leaf} , Eq. 2.4.8), and woody biomass (B'_{tree} , Eq. 2.4.5 - 2.4.7). The amount of N required (N_{req} , tonnes N) for this potential growth is then calculated as:

$$N_{req} = \begin{cases} (b_l B'_{leaf} - B_{leaf}) / CN_{ev} + & \text{evergreen species} \\ (B'_{tree} - B_{tree}) / CN_{stem}, & \\ B'_{leaf} / CN_{dec} + (B'_{tree} - B_{tree}) / CN_{stem}, & \text{deciduous species} \end{cases} \quad (2.4.17)$$

where b_l a conifer:deciduous leaf ratio parameter, set to 1.3, B'_{leaf} is the intermediate value for leaf biomass before calculating N limitation (tonnes C), B_{leaf} is the current leaf biomass (prior to this year's growth), CN_{ev} and CN_{dec} are the C:N ratios of evergreen and deciduous species, set to 60 and 40, respectively, B'_{tree} is the intermediate value for woody biomass, B_{tree} is the current woody biomass, and CN_{stem} is the C:N ratio of woody material, set to 450. The required N is then used to calculate an N availability ratio:

$$N_r = N_{avail} / \left(\frac{10000 N_{req}}{\text{plotsize}} \right) \quad (2.4.18)$$

where N_{avail} is plant-available N (tonnes N ha⁻¹, see Section 2.2.2), and plotsize is the plot area (in m²). This N availability ratio is used to calculate tree growth response to N availability as in Equation 2.4.14. The new actual diameter increment growth is then calculated as:

$$\delta DBH_{actual} = \delta DBH_{opt} f_{perm} \times \min(f_{gdd}, f_{drought}, f_{light}, f_N) \quad (2.4.19)$$

The updated tree DBH is then used to calculate new values for tree height (H), diameter at clear branch bole height (D_{cbb}), leaf biomass (B_{leaf}), and stem C and N weights (B_{tree} , B_{Ntree}). The amount of N in the tree is calculated as B_{tree}/CN_{stem} . The amount of N used in tree growth this year is calculated as:

$$N_{used} = \begin{cases} \delta B_{tree} / CN_{stem} + & \text{for evergreen species} \\ (b_l B'_{leaf} - B_{leaf}) / CN_{ev}, & \\ \delta B_{tree} / CN_{stem} + B_{leaf} / CN_{dec}, & \text{for deciduous species} \end{cases} \quad (2.4.20)$$

where δB_{tree} is the difference between the previous year's stem biomass and this year's stem biomass (tonnes C).

The actual DBH increment growth is also used to check for growth stress-related mortality. A tree has a potential for mortality given two checks: (1) The actual DBH increment growth is checked against a minimum DBH growth parameter, c_g (Eq. 2.4.21), and (2) the growth delimiter (i.e. $f_{lim} = f_{perm} \min(f_{gdd}, f_{drought}, f_{light}, f_N)$) is checked against a minimum growth threshold, δDBH_{min} , set to a default value of 0.03 cm.

$$c_g = \min\left(\frac{DBH_{max}}{0.1AGE_{max}}, \delta DBH_{min}\right) \quad (2.4.21)$$

If $\delta DBH_{actual} \leq c_g$ or if $f_{lim} \leq \delta DBH_{min}$ then the tree's mortality counter (m_{count}) is increased by 1. If this value reaches 2 (i.e. if the tree experiences low growth or stressful conditions for 2 consecutive years), the tree is flagged for potential growth stress-related mortality (Section 2.5.1). Otherwise, m_{count} is (re)set to 0 and no stress flag is added.

The N used by tree growth on the plot is subtracted from the overall available N (tonnes N ha⁻¹; $N_{avail} = \max(N_{avail} - \frac{10000}{plotsize}N_{used}, 0.0)$, where $plotsize$ is plot area in m²) and used in the regeneration subroutine (Section 2.6) to determine whether and how many new trees may be established.

Lower Branch Thinning

UVAFME also checks for stress-induced lower branch thinning, which would increase the clear branch bole height (H_{cbb}). If $f_{lim} \leq \delta DBH_{min}$, then lower branch thinning occurs via an increase in H_{cbb} at a rate of 1.01 m in height. H_{cbb} is increased by 1.01 m (checking first to make sure this would not cause $H_{cbb} > H$), and then updated values for D_{cbb} and B_{tree} are calculated.

The litterfall from this branch thinning is added to the appropriate litter cohort pools (i.e. genus-specific leaf litter, and twig, stem, and root litter; Section 2.2.2).

2.5 Tree Mortality

Trees in UVAFME may die from stress- or age-related factors (Section 2.4.3) or from disturbances by wildfire, windthrow, and bark beetles (Foster, Shuman, Shugart, & Negron, 2018; Shuman et al., 2017; Foster et al., 2017). Currently, fire and windthrow occurrence are probabilistic, based on site-specific input mean return intervals. If no fire or windthrow disturbance

occurs on the plot, only mortality from low growth, age, or insect infestation is considered.

2.5.1 Growth Stress or Age

Stress

Trees that had a potential mortality flag from prolonged low growth or stress (Section 2.4.3) are checked for stress-related mortality via an input species-specific stress tolerance parameter. A uniform random number between 0 and 1 (see Section 2.7) is generated and checked against c_{stress} , which ranges from 0.21 to 0.33 depending on the input stress tolerance (1-5; 1: high tolerance, 5: low tolerance). If the random number is below c_{stress} then the tree is set to die from low growth.

Age

Trees also have a chance of dying each year based on the input species-specific probability of reaching its maximum age. Again, a random uniform number between 0 and 1 is checked against a parameter, $p_{max} = 1 - e^{-k_{age}/AGE_{max}}$, where k_{age} is a parameter equalling 4.605, 6.908, or 11.51, depending on the species-specific age parameter (1-3; 1: high probability of reaching AGE_{max} , 3: low probability of reaching AGE_{max}). These parameters are based on a tree having a 1%, 0.1%, and 0.0001% chance of reaching the tree species' average maximum age (Shugart & Seagle, 1985; Botkin et al., 1972).

If the random number is below p_{max} then the tree is set to die from random mortality. It is important to note that p_{max} does not change with individual tree age, but is only related to a tree species' average maximum age and its probability of reaching that age.

Litter

Trees that die and the associated litter is placed in appropriate litter cohorts for decomposition (Section 2.2.2). Leaf litter biomass (B_{leaf}/c , $c = 0.45$, tonnes) is added to a genus-specific annual litter pool, M_{gen} . Twig litter (B_{twigs}/c) is added to a twig litter (M_{twigs} , tonnes) pool, and root litter (B_{roots}/c) is added to a root litter pool (M_{roots} , tonnes). If the tree's DBH is below 10 cm, the stem biomass (B_{bole}/c) is added to a small wood litter pools (M_{Swood} , tonnes), otherwise it is added to a large wood litter pool (M_{Lwood} , tonnes).

If the tree does not die, the amount of annual litter is calculated as:

$$M_{leaves} = \begin{cases} B_{leaf}(1 - b_l)/c, & \text{for evergreen species} \\ B_{leaf}, & \text{for deciduous species} \end{cases} \quad (2.5.1)$$

where b_l is a coniferous leaf area ratio parameter, set to 1.3.

2.5.2 Disturbances

Fire and windthrow disturbances are based on site-specific input return intervals. Each plot run for a specific site has a probability of fire ($p_{fire} = 1/FRI$) or windthrow ($p_{wind} = 1/WRI$) occurring each year, independent from other plots and other sites. Fire probability is additionally connected to climate via an aridity index: $AI = P/PET$ (Feng & Fu, 2013), where P is annual precipitation (cm) and PET is annual potential evapotranspiration (cm). The first ten years of simulation are used to calculate a base/historical value for AI , AI_{base} . In subsequent years, the base aridity index is compared to the current year's aridity index to modify the fire probability as:

$$f'_{prob} = \begin{cases} f_{prob} + f_{prob} \left(\frac{AI_{base} - AI}{AI_{base}} \right), & AI < AI_{base} \\ f_{prob} - f_{prob} \left(\frac{AI - AI_{base}}{AI_{base}} \right), & AI > AI_{base} \end{cases} \quad (2.5.2)$$

Once a fire or windthrow event occurs, individual tree mortality is based on litter and site conditions (for fire), as well as tree size- and species-specific tolerances (Section 2.5.2).

Fire

If a fire occurs, the amount of litter and the moisture conditions on the plot are used to calculate the scorch height and crown scorch- and cambial damage-related mortality of each individual tree. Based on equations from Schumacher et al. (2006), the crown scorch (CS, %) of each tree is calculated as:

$$CS = \begin{cases} 100.0(ck_1 + ck_2DBH)f_{av}, & DBH < 40 \\ 100.0(ck_1 + ck_2DBH_{eff})f_{av}, & DBH \geq 40 \end{cases} \quad (2.5.3)$$

where ck_1 and ck_2 are parameters from Schumacher et al. (2006), set to 0.21111 and -0.00445, $DBH_{eff} = 40$ cm, and f_{av} is the available fuel for wildfire (tonnes ha^{-1}). The available fuel is based on the amount of leaf, twig, and bole litter (Section 2.2.2). As in Schumacher et al. (2006) and Bonan (1989), all leaf litter and all moss litter (M_l , t ha^{-1}) is assumed to be

available for burning. Twig fuel is based on the twig litter amount as well as plot-level moisture conditions:

$$f_{twigs} = (tfc_1 + tfc_2 DI_u)(M_{twigs}) \quad (2.5.4)$$

where tfc_1 and tfc_2 are parameters from Schumacher et al. (2006), set to 0.8 and 0.2, DI_u is a drought index, calculated using the percentage of the growing season with high atmospheric demand and low soil moisture (Section 2.4.2), and M_{twigs} is the weight of twig litter on the plot (tonnes ha^{-1}). Small bole ($DBH \leq 10.0$ cm) fuel is calculated using the same equation as with twig litter:

$$f_{Sboles} = (tfc_1 + tfc_2 DI_u)(M_{Sboles}) \quad (2.5.5)$$

where M_{Sboles} is the weight of dead stems smaller than 10 cm DBH on the plot (tonnes ha^{-1}). Large bole ($DBH > 10.0$ cm) fuel is calculated as:

$$f_{Lboles} = bfc DI_u M_{Lboles} \quad (2.5.6)$$

where bfc is a parameter from Schumacher et al. (2006), set to 0.4, and M_{Lboles} is the weight of dead stems larger than 10 cm DBH on the plot (tonnes ha^{-1}). Total available fuel for burning (f_{av} , tonnes ha^{-1}) is then calculated as:

$$f_{av} = M_l + f_{twigs} + f_{Sboles} + f_{Lboles} \quad (2.5.7)$$

Using the crown scorch (CS), tree size, and a species-specific bark thickness parameter (cm bark $cm DBH^{-1}$), the probability of fire mortality is calculated for each tree as (Schumacher et al., 2006):

$$p_{mfire} = \left(1 + e^{-1.466 + 1.91(b_{thick}DBH) - 0.1775(b_{thick}DBH^2) - 0.00541CS^2} \right)^{-1} \quad (2.5.8)$$

A random uniform number between 0.0 and 1.0 (Section 2.7) is generated, and if this value is below p_{mfire} , the tree is marked for mortality by fire.

Live Tree Consumption

Trees that die from fire are assumed to burn in proportion to site moisture conditions. The proportion of live roots that is consumed is calculated using an equation adapted from Bonan (1990):

$$cons_{roots} = \max \left[0.0, \min \left(0.302 + 0.597DI_{fc} + 3.34(d_{moss} + d_{org}), 0.9 \right) \right] \quad (2.5.9)$$

where d_{moss} and d_{org} are the depths of the moss and organic layer (m), DI_{fc} is a drought index related to the site drainage conditions and the minimum volumetric moisture content that year:

$$DI_{fc} = \max \left(0.0, \frac{m_{sat} - m_{min}}{m_{sat} - m_{pwp}} \right) \quad (2.5.10)$$

where m_{sat} is the mineral layer saturation capacity, m_{pwp} is the mineral layer permanent wilting point, and m_{min} is the minimum moisture content that year (volumetric) (Section 2.2.1).

The proportion of live branches that burns is set to 0.1, as in Schumacher et al. (2006). The proportion of live bole that burns is set to 0.05, and the proportion of live foliage that burns is 0.5 (Schumacher et al., 2006; Fahnestock & Agee, 1983). The unburned portions of the tree are placed into the appropriate litter cohorts as with tree mortality from growth or age stress.

If the tree does not die by fire, annual litterfall is calculated as previously (Eq. 2.5.1).

Litter Consumption

When a fire occurs the litter and humus layers are also consumed. All decaying cohorts of root litter, bole litter, and twig litter are consumed at the same rates as calculated previously (Eq. 2.5.4 - 2.5.6; 2.5.9). The proportion of well-decayed wood litter that is burned is calculated using an equation adapted from Bonan (1990)

$$cons_{WDW} = \max \left(0.0, \min \left(0.098 + 0.597DI_{fc} + 3.34(d_{moss} + d_{org}) \right), 0.5 \right) \quad (2.5.11)$$

The proportion of live moss and humus that is burned is also calculated using an equation adapted from Bonan (1990):

$$cons_{org} = \max \left(0.0, \min \left(0.079 + 0.5744DI_{fc} + 3.34(d_{moss} + d_{org}) \right), 0.658 \right) \quad (2.5.12)$$

All moss litter and leaf litter is assumed to burn at 100%. Burning litter and live biomass also volatilizes some amount of nitrogen, which then becomes available for plant use. This N volatilization is assumed to be proportional to the percentage of N in the litter or plant component as well as to moisture conditions and organic/moss depth:

$$pN_{vol} = 1 - \max(0.0, \min(0.6426DI_{fc} + 3.34(d_{moss} + d_{org})), 0.7) \quad (2.5.13)$$

and

$$N_{vol} = M_{cons} \times pN_{vol} \times pN \quad (2.5.14)$$

where pN_{vol} is the proportion of N volatilized, M_{cons} is the mass of litter/live biomass that is consumed by fire, pN is the proportion of that weight that is nitrogen, and N_{vol} is the mass of N volatilized (tonnes N). This volatilized N is made available for plant use and added to the plant-available N pool (Section 2.2.2, 2.4.2).

Windthrow

As with fire occurrence, windthrow is also probabilistic, based on a site-specific input wind return interval (WRI). For each plot simulated and each year, a uniform random number between 0 and 1 is generated and if this value is below the wind probability ($p_{wind} = 1/WRI$) then a windthrow event occurs on the plot that year, independent from other plots or sites. The probability of windthrow mortality of each individual tree on the plot is based on tree size (Rich et al., 2007) (Fig 2.41):

$$p_{mwind} = \left(1.0 + e^{-0.75 \ln(DBH)}\right)^{-1} \quad (2.5.15)$$

The components of trees that die by windthrow are added to the appropriate litter cohorts as with mortality from age- or growth-related stress. If the tree does not die, annual litterfall is calculated as above (Eq. 2.5.1).

Insects

UVAFME is also able to simulate mortality from the spruce beetle (*Dendroctonus rufipennis* (Kirby)), a bark beetle which infests spruce (*Picea* spp.) species. Mortality is simulated as the probability of infestation of each host tree based on climate-, site-, and tree-level characteristics (Foster et al., 2018).

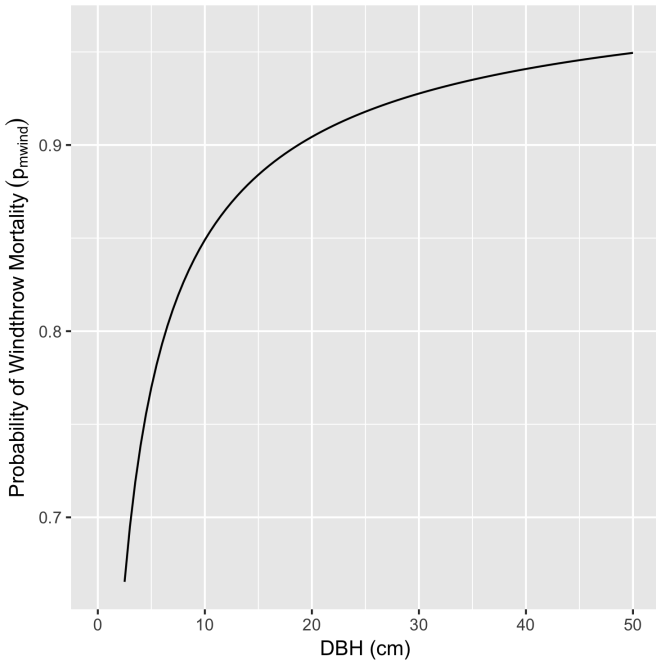


Figure 2.41: Probability of windthrow mortality with increasing tree DBH (Eq. 2.5.15) (Rich et al., 2007).

Climate factors for this submodel were derived from studies on the phenology of spruce beetles and what influences their shift from a semivoltine to a univoltine life cycle (Hansen et al., 2001; Sherriff et al., 2011; Hansen et al., 2011). Based on a detailed spruce beetle phenology study by Hansen et al. (2001), calculations were included to determine whether the beetle population on each plot has a semivoltine (two-year) or univoltine (one-year) life cycle. This calculation is based on the cumulative hours above 17°C during the period of 40 to 90 days prior to the beetles' peak flight. Cumulative hours above 17°C during this period are calculated using a sinusoidal temperature formula from Reicosky et al. (1989) (Section 2.1; Eq. 2.1.7). This equation is then used to accumulate the number of hours above 17°C (H_{17}) during 40 to 90 days prior to peak spruce beetle flight. Cumulative hours above 17°C is equal across all plots within an individual site, but may change from year to year and from site to site. The probability of any one plot having beetles with a univoltine life cycle (p_{uv} ; Eq. 2.5.16; Fig 2.42), from Hansen et al. (2001), is then calculated and is used to influence the infestation probability of each individual tree on that plot.

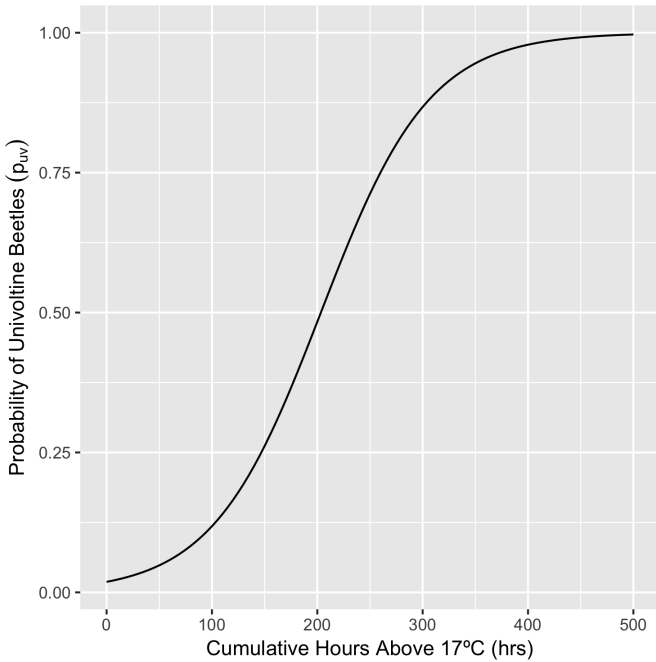


Figure 2.42: Probability of univoltine (one year life cycle) beetle populations with cumulative hours above 17°C during the period between 40 and 90 days prior to peak beetle flight (Eq. 2.5.16) (Hansen et al., 2001).

$$p_{uv} = \left(1.0 + e^{3.954 - 0.01944 H_{17}} \right)^{-1} \quad (2.5.16)$$

Plot-level factors are calculated each year based on individual plot characteristics, and thus will vary between the simulated plots at a given site. These plot-level factors are based on spruce beetle susceptibility stand ratings from Schmid and Frye (1976). As in their stand rating system, this model uses average DBH of live spruce above 25.4 cm DBH, plot-level spruce basal area, and percent of spruce in the canopy as factors for determining plot-wide susceptibility to spruce beetle attacks. Depending on the value of each of the three factors, each plot receives three factor ratings from 1 to 3 (Table 2.4), and the ratings from each individual factor are added together to produce an overall stand rating (possible values being 3 to 9).

The overall stand rating is then used to calculate the probability for spruce beetle infestation in each tree due solely to plot characteristics (f_{stand} , 0 to 1; Eq. 2.5.17; Fig. 2.43). This stand-level probability is utilized to calculate the individual-tree infestation probability (Eq. 2.5.20) and is the same for every tree on the same plot in a given year.

Table 2.4: Values of plot factors associated with each factor rating used to calculate overall plot-wide susceptibility to spruce beetle infestation from Schmid and Frye (1976).

Plot Factor Value			
Susceptibility Rating	Basal area of spruce in the stand ($\text{m}^2 \text{ ha}^{-1}$)	Mean DBH of live spruce over 24.5 cm DBH (cm)	Percent spruce in canopy (%)
Low (1)	< 22.95	< 30.48	< 50
Medium (2)	22.95 to 34.43	30.48 to 40.64	50 to 65
High (3)	≥ 34.43	≥ 40.64	≥ 65

$$f_{stand} = 0.75 \ln(f_{BA} + f_{DBH} + f_{can}) - 0.8 \quad (2.5.17)$$

where f_{BA} is the factor rating from column one, f_{DBH} is the factor rating from column two, and f_{can} is the factor rating from column three of Table 2.4. This overall stand rating is then modified based on recent windthrow events to account for the high influence of blowdown on bark beetle outbreaks (Christiansen et al., 1987; Wichmann & Ravn, 2001; Mezei et al., 2014). Following a windthrow event, the overall stand infestation probability is increased by 0.3 for the first three years, 0.2 from four to six years, and 0.1 from five to nine years. Because spruce beetle populations can utilize downed spruce trees (from windthrow or other mortality factors) for reproduction at low levels (Schmid & Frye, 1977), plot-wide susceptibility is also influenced based on the amount of coarse woody debris on the plot available for spruce beetle colonization. Spruce trees larger than 25.4 cm DBH that die from either windthrow, age, or low growth are added to a pool of coarse woody debris (CWD_{spruce} , tonnes C ha^{-1}). A plot-wide woody debris factor (f_{cwd} , 0 to 1) is then calculated, which increases linearly with increasing spruce woody debris:

$$f_{cwd} = \min\left(\frac{CWD_{spruce}}{CWD_{base}}, 1.0\right) \quad (2.5.18)$$

where CWD_{base} is set to 300 tonnes C ha^{-1} , corresponding to potential coarse woody debris that may occur from a very severe windthrow event, as in Temperli et al. (2013). Spruce coarse woody debris decays as with other large boles (Section 2.2.2).

Tree-level factors that affect the probability of spruce beetle infestation include individual tree size (f_{tDBH}), stress level (f_{stress}), and scorch volume from recent fires (f_{scorch}). Under normal conditions, trees that are smaller

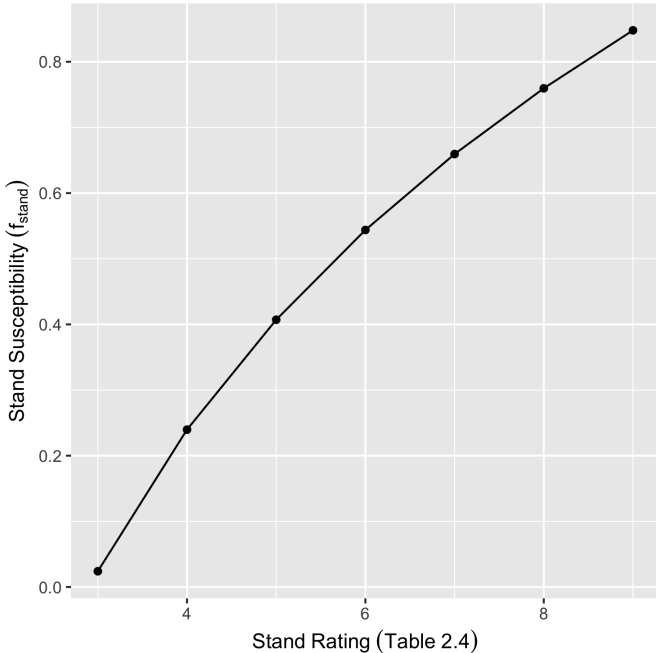


Figure 2.43: Stand susceptibility with increasing stand ratings from Table 2.4. Stand ratings are derived from Schmid and Frye (1976).

than 30 cm DBH are not susceptible to spruce beetle attack (DeRose & Long, 2012). Under epidemic conditions (i.e. greater than $10 \text{ m}^2 \text{ ha}^{-1}$ of basal area killed per year) trees as small as 10 cm DBH may be killed by spruce beetles (Peet, 1981; Veblen et al., 1994; DeRose & Long, 2012). Otherwise, based on information from relevant literature on bark beetle infestations (Furniss et al., 1979; Negron, 1998; Hood & Bentz, 2007; Zolubas et al., 2009; Mezei et al., 2014) and inventory data from the US Forest Service, infestation probability due to tree size (f_{tDBH} , 0 to 1) increases linearly with increasing tree diameter (Eq. 2.5.19).

$$f_{tDBH} = \min(0.011DBH, 1.0) \quad (2.5.19)$$

Many studies have shown that prolonged stress and associated low tree vigor, due to drought, age, or other factors, increases a tree's susceptibility to bark beetle attacks (Kalkstein, 1976; Waring & Pitman, 1980; Larsson et al., 1983; Christiansen et al., 1987; Mattson & Haack, 1987; Malmstrom & Raffa, 2000; McKenzie et al., 2009). In this model, tree stress is quantified as prolonged low diameter increment growth (i.e. less than 0.03 cm per year). Probability of spruce beetle infestation due to stress level (f_{stress} , 0 to 1) increases by 0.1 each year the tree in question has diameter growth

below 0.03 cm, and is reset to 0 if the tree has higher than 0.03 cm growth in any given year. Damage due to fire has also been cited as a potential precursor to bark beetle attack (Geiszler et al., 1984; Christiansen et al., 1987; Rasmussen et al., 1996; Hood & Bentz, 2007). UVAFME calculates fire damage by percent crown volume scorched (CS , %) based on fire dynamics equations from Keane et al. (2011) and Schumacher et al. (2006) (see above Fire section). In this spruce beetle model, susceptibility to beetle infestation based on fire damage (f_{scorch} , 0 to 1) is equal to the proportion of crown volume scorched by wildfire.

As with the individual plot-level factors, these tree-level factors are combined, along with the overall plot-wide factors, to produce an overall tree-level susceptibility to spruce beetles (f_{tree} , 0 to 1; Eq. 2.5.20).

$$f_{tree} = \min \left(0.3f_{stand} + 0.25f_{tDBH} + 0.2f_{stress} + 0.1f_{scorch} + 0.4f_{cud}, 1.0 \right) \quad (2.5.20)$$

Coefficients associated with each susceptibility factor are based on susceptibility ratings from relevant literature (Schmid & Frye, 1976; Seidl et al., 2007; Hart et al., 2014). This susceptibility is used to calculate the final tree-level probability for spruce beetle infestation (Eq. 2.5.21, Fig. 2.44):

$$p_{beetle} = 1.0 - e^{(-2.0f_{tree}^{1.3})^{gen}} \quad (2.5.21)$$

where gen is equal to 1.8 if the plot in question has univoltine beetles (based on uniform random number draws compared to the probability for univoltinism - p_{uv} ; Eq. 2.5.16) and 0.5 if it does not. Equation 2.5.21 was adapted from a bark beetle modeling study by Seidl et al. (2007) on the European spruce bark beetle in Norway spruce forests.

Once a tree becomes infested by spruce beetles, it ceases growth (i.e. $\delta DBH_{actual} = 0.0$ - see Section 2.4.3) (Frank et al., 2014), and loses its needles after two years (i.e. $LA = 0.0$ - see Section 2.4.1) (Schmid & Frye, 1977). Finally, after five years of being infested, the tree is set to fall and its component parts are added to the appropriate litter cohorts for decomposition (Section 2.2.2). A study by Hart et al. (2014) found that proximity to infested spruce trees was an important factor in determining infestation probability. Thus, within this spruce beetle submodel, during the time when a tree is infested and still on a plot it increases the infestation probability of directly (by 0.3) and diagonally (by 0.1) adjacent spruce trees on the same plot (see Section 2.6.2 for more on tree positions).

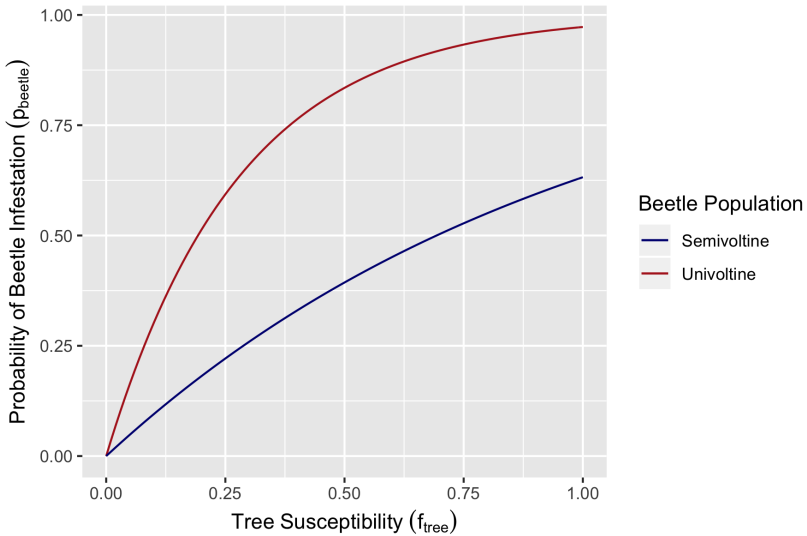


Figure 2.44: Probability of beetle infestation increases with increasing tree susceptibility (f_{tree} , Eq. 2.5.20) and with univoltine beetle populations (Eq. 2.5.21).

2.6 Tree Regeneration

Annual establishment of new trees in UVAFME is based on the species-specific seed and seedling banks on each plot as well as the current environmental conditions and species-specific tolerances. Similar to other gap models, the species of each new tree established is determined stochastically, weighted by each species' ability to survive in the current plot's environment. The seedbank and seedling bank of each species is additionally modified to account for seeding strategies (i.e. serotiny, sprouting etc.) and natural mortality of seeds and seedlings (Yan & Shugart, 2005).

New trees are only established if the available N (N_{avail}) is still above 0 tonnes N ha⁻¹ from N use in annual tree growth (Section 2.4.3). If there is any available N, a species-specific regrowth variable ($r_{new_{sp}}$, 0 to 1) is calculated based on the current environmental conditions and species-specific tolerances:

$$r_{new_{sp}} = f_{perm} f_{gdd} f_{drought} f_{light} f_N \quad (2.6.1)$$

This regrowth variable is additionally modified to account for the amount of reproductively mature trees on the plot. For each species, if any trees of that species are older than the minimum age for reproduction (default of 10 years for most species) then $r_{new_{sp}}$ is not modified. Otherwise, $r_{new_{sp}}$ is multiplied by 0.50 as in Bonan (1989). Finally, if $r_{new_{sp}}$ is at or below the

minimum growth threshold (δDBH_{min}) then it is set to 0.0, otherwise no change is applied. The maximum regrowth variable ($r_{new_{max}}$, 0 to 1) is set as the maximum value of $r_{new_{sp}}$ across all species.

These values are used to calculate total number of trees to renew this year:

$$nr_{max} = \min \left(nt_{max} r_{new_{max}} - nt, nt_{max} \right) \quad (2.6.2)$$

and

$$nr = \min \left(\max(nr_{max}, 3), nt_{max} - nt \right) \quad (2.6.3)$$

where nr_{max} is the maximum amount of renewable trees, nt is the current number of trees on the plot, nt_{max} is the maximum number of trees allowed on a plot and nr is the number of trees to be renewed this year.

2.6.1 Seed and Seedling Banks

The species of each tree to be established is determined using annual modifications to species-specific seed and seedling banks. The seedbank for each species (seeds m^{-2}) is updated as:

$$S_{bank} = S_{bank} + inv + s_{num} sp_{avail} \quad (2.6.4)$$

where inv is a species-specific input parameter indicating the number of seeds from outside the plot (seeds m^{-2}), with wind dispersed seeds generally have an inv value of 1.0; s_{num} is a species-specific input parameter indicating the number of seeds that could be produced from within the plot (seeds m^{-2}); and sp_{avail} is a variable indicating the presence and reproduction ability of each species on the plot (Eq. 2.6.5).

$$sp_{avail} = \begin{cases} 1.0, & \text{if any } DBH_{t_{sp}} - DBH_{max_{sp}} \delta DBH_{min} > 0.0 \\ 0.0, & \text{otherwise} \end{cases} \quad (2.6.5)$$

where $DBH_{t_{sp}}$ is the DBH of any tree of species sp and $DBH_{max_{sp}}$ is the average maximum DBH of species sp . The seedbank is additionally modified to incorporate the effects of fire (if fire occurred that year):

$$S_{bank} = S_{bank} k_{fire} \quad (2.6.6)$$

where k_{fire} is a parameter ranging from 0.001 to 1000, depending on the input species-specific regeneration tolerance to fire - ranging from 1 (fire is very beneficial to regeneration) to 5 (fire is very detrimental to regeneration).

If the species-specific regrowth variable calculated above ($r_{new_{sp}}$, Eq. 2.6.1) is greater than δDBH_{min} , then all seeds in the seed bank are moved to the species' seedling bank and the seedbank is set to 0.0. Otherwise, no seeds are added to the seedling bank and the seedbank is multiplied by the species-specific parameter NDS , which represents the annual percentage loss of seeds for each species.

As in Bonan (1990) and Bonan and Korzukhin (1989), if seeds are added to the seedling bank, it is then modified by a variable related to the depths of the organic and moss layers, d_{org} and d_{moss} (m, Sections 2.2.2 and 2.3):

$$f_{org} = \begin{cases} e^{-7.4(d_{org}+d_{moss})}, & tol_{org} = 1 \\ e^{-52.4(d_{org}+d_{moss})}, & tol_{org} = 2 \end{cases} \quad (2.6.7)$$

where tol_{org} is a species-specific organic/moss layer depth tolerance parameter (1: tolerant; 2: intolerant). This value is multiplied by the seedling bank number (SL_{bank}). The above equation was modified from Bonan and Korzukhin (1989) using data on post-fire seedling counts from Johnstone et al. (2010). The seedling bank is then additionally modified to account for layering and sprouting. If the combined depths of the organic and moss layers is greater than 5 cm, and the species is able to reproduce by layering, the species' seedling bank is multiplied by 1.8 as in Bonan (1989).

If the species is able to produce sprouts, the species' seedling bank is updated as: $SL_{bank} = SL_{bank} + n_{sprouts} s_{pavail}$, where $n_{sprouts}$ is a species-specific input parameter indicating how many sprouts per tree the species can produce.

2.6.2 Tree Establishment

New trees are generated using the total number of trees to be established (nr , Eq. 2.6.3), as well as the size of each species' seedling bank and each species' regrowth variable ($r_{new_{sp}}$, Eq. 2.6.1). Each species' seedling bank is converted from seedlings m^{-2} to seedlings $plot^{-1}$ and used to calculate a species-specific establishment variable, e_{sp} (seedlings $plot^{-1}$):

$$e_{sp} = SL_{bank} r_{new_{sp}} \quad (2.6.8)$$

Each individual e_{sp} value is summed across all species to calculate an overall e_{sum} value. Each species' e_{sp} value is converted to a relative/probability of establishment parameter: $e_r = e_{sp}/e_{sum}$ (0 to 1), and then to a cumulative probability parameter (e_c , 0 to 1).

Subsequently, nr trees are renewed, and for each tree the species is determined by random uniform draws compared to the cumulative establishment

probability. Once a species is determined, the seedling bank for that species is decreased by one.

Trees in UVAFME are located on a grid (generally 30×30). Currently, trees within the same plot interact spatially with one another with respect to insect infestation (Section 2.5.2). When a new tree is established, its x/y location on the grid is drawn randomly from the set of empty grid spaces on the plot. The tree then carries this same grid cell location throughout its lifetime until its death, at which point that grid cell is once again empty.

New trees that are established are assigned a random DBH via: $DBH = 1.5 + r$, where r is a normally distributed random number (mean = 0.0; sd = 1.0). The new tree's DBH is restricted to be values between 0.5 and 2.5 cm. The tree's clear branch bole height (H_{cbb} , m) is set to 1.0 m, and all other tree allometric characteristics (height, diameter at clear branch bole height, and biomass) are calculated using equations from Section 2.4.1.

Annual litter from newly established trees is calculated as with equation 2.5.1. After all new trees have been established and decremented from the relevant species' seedling bank, each species seedling bank is updated and converted back to seedlings m^{-2} as:

$$SL_{bank} = \frac{SL_{bank}NDE}{plotsize} \quad (2.6.9)$$

where NDE is a species-specific input parameter representing the percentage annual loss of seedlings.

2.7 Random Processes

Stochasticity is incorporated throughout UVAFME in the climate, (Section 2.1), mortality (Section 2.5), and regeneration (Section 2.6) subroutines via pseudorandom number generators.

2.7.1 Random Number Seeds

Random number generator seeds are used in the pseudorandom number generators. In this version, the seed can be fixed across all sites run (*fixed_seed* = TRUE) or it can be different for each site. If the seed is fixed, the seed is reset for each site. Using the same seed ensures reproducibility (i.e. the same random numbers are generated each time the same site is run).

If *fixed_seed* = TRUE, the default seed or a user-supplied seed is used at the beginning of each site's run to set up the number generators. If *fixed_seed* = FALSE and no seed is supplied, new seeds are used for each

site. In this case, the Fortran intrinsic function **date_and_time** is used to get the milliseconds of the current second (*idate*). The Fortran intrinsic **random_seed** is then used to get a random seed (*iseed*). This value is then modified as:

$$iseed = \begin{cases} iseeds \times idate, & iseeds \neq 0 \\ default_seed \times idate, & iseeds = 0 \end{cases} \quad (2.7.1)$$

where *default_seed* is a default integer seed (size 7) within the model. This seed is set as the random number seed for subsequent random number calls.

2.7.2 Pseudorandom Number Generators

Four different pseudorandom number generators are used in the model: a uniform random number generator, a normally distributed random number generator, and two climate variable-specific uniform and normally distributed random number generators. The climate variable-specific generators are only used in creating the monthly and daily values of temperature, precipitation, and cloud cover from their input distributions. The other two generators are used for all other random number calls.

Uniform Random Numbers

The climate-specific uniform random number generator is created using a linear congruent method with a shuffle (Press et al., 1989). The regular uniform random number generator (i.e. for all uniform random calls *except* climate variables) uses the Fortran intrinsic function **random_number** to generate a uniform random number. This generator uses two separate congruential generators and produces a period of 10^{18} (L'ecuyer, 1988; Bratley et al., 1987).

For both generators, the uniform random number is then modified as:

$$urand = lb + (ub - lb)urand \quad (2.7.2)$$

where *lb* and *ub* are lower and upper bounds for the number, respectively, default to *lb* = 0.0 and *ub* = 1.0. Both generators show pseudorandom results with a uniform distribution [0, 1] (Fig. 2.45).

Random Normals

The climate-specific normally distributed random number generator uses the climate-specific uniform random number generator and the Box-Muller polar

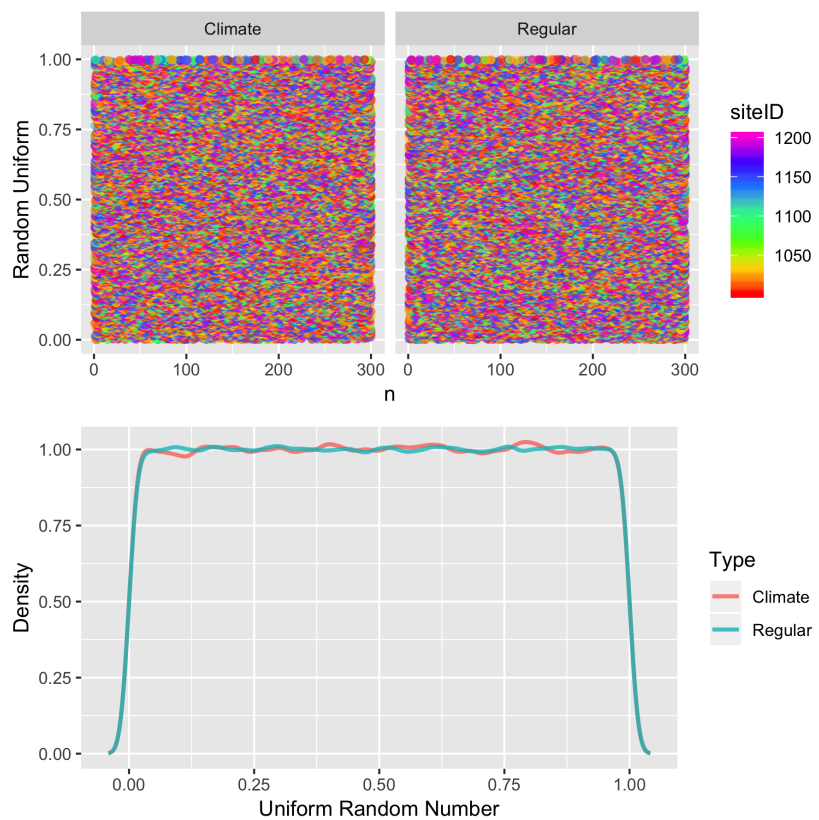


Figure 2.45: Example simulation of uniform random numbers using the regular and climate-specific pseudorandom number generators ($n = 2333100$, $\text{mean}_{\text{clim}} \approx 0.5004$, $\text{mean}_{\text{reg}} \approx 0.5002$, $\text{sd}_{\text{clim}} \approx 0.2884$, $\text{sd}_{\text{reg}} \approx 0.2887$; σ of a uniform distribution $= \sqrt{\frac{(lb-ub)^2}{12}}$, ≈ 0.2887 when $lb = 0.0$ and $ub = 1.0$).

method to generate a normally distributed random number with a specified mean and standard deviation (default to mean = 0.0, sd = 1.0). Two random uniforms are generated between -1 and 1 and these values are used to calculate:

$$w = \sqrt{\frac{-2.0 \ln(urand_1^2 + urand_2^2)}{urand_1^2 + urand_2^2}} \quad (2.7.3)$$

where $urand_1^2 + urand_2^2$ must not equal 0.0 or be greater than 1.0. The random normal is then calculated as:

$$nrand = (urand_1 w)sd + mn \quad (2.7.4)$$

where mn and sd are the input/default mean and standard deviation. The regular normally distributed random number generator also uses the Box-Muller polar method, but with the regular uniform random number generator to generate the initial two random uniforms. Both generators show pseudorandom results with a normal distribution (mean = mn , standard deviation = sd) (Fig 2.46).

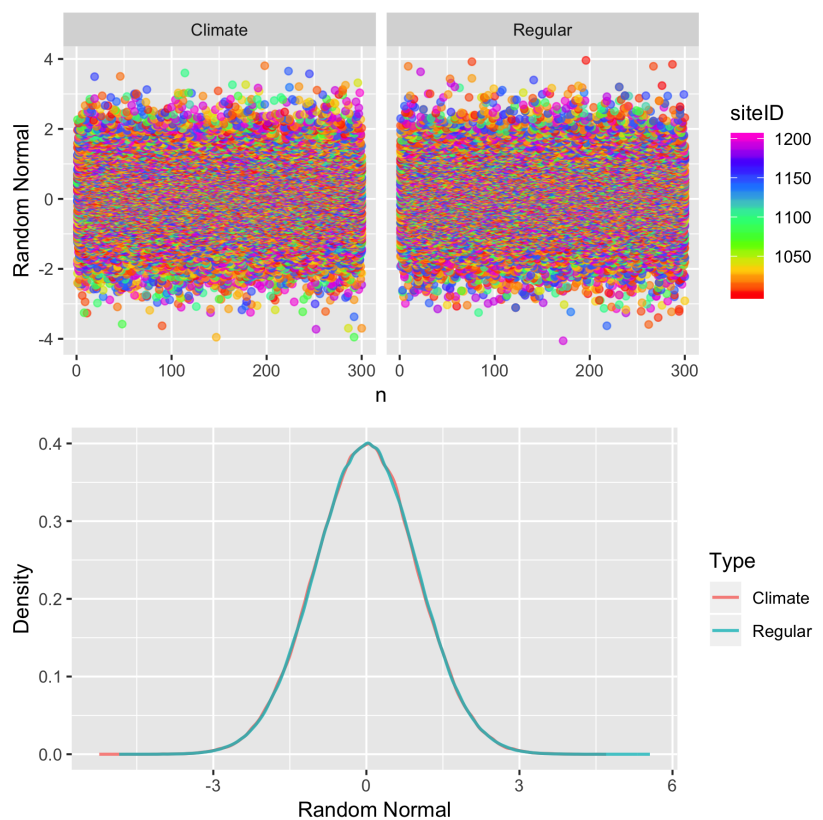


Figure 2.46: Example simulation of normally distributed random numbers using the regular and climate-specific pseudorandom number generators ($n = 2333100$, $\text{mean}_{\text{clim}} \approx -0.0042$, $\text{mean}_{\text{reg}} \approx -0.00044$, $\text{sd}_{\text{clim}} \approx 1.002$, $\text{sd}_{\text{reg}} \approx 1.0002$).

References

- Bonan, G. (1989). A computer model of the solar radiation, soil moisture, and soil thermal regimes in boreal forests. *Ecological Modelling*, 45, 275–306.
- Bonan, G. (1990). Carbon and nitrogen cycling in North American boreal forests I. Litter quality and soil thermal effects in interior Alaska. *Biogeochemistry*, 10, 1–28.
- Bonan, G., & Korzukhin, M. (1989). Simulation of moss and tree dynamics in the boreal forests of interior Alaska. *Vegetatio*, 84, 31–44.
- Bosen, J. (1960). A formula for approximation of the saturation vapor pressure over water. *Monthly Weather Review*, 88, 275–276.
- Botkin, D. (1993). *Forest Dynamics: An Ecological Model*. New York, NY: Oxford University Press.
- Botkin, D., Janak, J. F., & Wallis, J. R. (1972, November). Some Ecological Consequences of a Computer Model of Forest Growth. *The Journal of Ecology*, 60(3), 849. Retrieved 2015-10-19, from <http://www.jstor.org/stable/2258570?origin=crossref> doi: 10.2307/2258570
- Bratley, P., Fox, B., & Schrage, L. (1987). *A Guide to Simulation* (2nd ed.). New York, N.Y..
- Brock, T. (1981). Calculating solar radiation for ecological studies. *Ecological Modelling*, 14, 1–19.
- Campbell, G. (1977). *An Introduction to Environmental Biophysics*. New York, NY: Springer.
- Christiansen, E., Waring, R., & Berryman, A. (1987). Resistance of conifers to bark beetle attack: searching for general relationships. *Forest Ecology and Management*, 22, 89–106.
- DeRose, R., & Long, J. (2012). Drought-driven disturbance history characterizes a southern Rocky Mountain subalpine forest. *Canadian Journal of Forest Research*, 42, 1649–1660.
- DeWalle, D., Henderson, Z., & Rango, A. (2002). Spatial and temporal variations in snowmelt degree-day factors computed from snotel data in the upper Rio Grande Basin. *Western Snow Conference 2002*, 73–

81.

- Emanuel, W., West, D., & Shugart, H. (1978). Spectral analysis of forest model time series. *Ecological Modelling*, 4, 313–326.
- Fahnestock, G., & Agee, J. (1983). Biomass consumption and smoke production by prehistoric and modern forest fires in western Washington. *Journal of Forestry*, 81, 653–656.
- Feng, S., & Fu, Q. (2013). Expansion of global drylands under a warming climate. *Atmospheric Chemistry and Physics*, 13, 10081–10094.
- Foster, A., Shugart, H., & Shuman, J. (2015). Model-based evidence for cyclic phenomena in a high-elevation, two-species forest. *Ecosystems*, 19(3), 437–449. doi: 10.1007/s10021-015-9945-y
- Foster, A., Shuman, J., Shugart, H., Dwire, K., Fornwalt, P., Sibold, J., & Negron, J. (2017). Validation and application of a forest gap model to the southern Rocky Mountains. *Ecological Modelling*, 351, 109–128.
- Foster, A., Shuman, J., Shugart, H., & Negron, J. (2018). Modeling the interactive effects of spruce beetle infestation and climate on subalpine vegetation. *Ecosphere*, 9(10), e02437.
- Frank, J. M., Massman, W. J., Ewers, B. E., Huckaby, L. S., & Negrón, J. F. (2014, June). Ecosystem CO₂/H₂O fluxes are explained by hydraulically limited gas exchange during tree mortality from spruce bark beetles: CO₂/H₂O FLUX EXPLAINED FROM DISTURBANCE. *Journal of Geophysical Research: Biogeosciences*, 119(6), 1195–1215. Retrieved 2015-10-19, from <http://doi.wiley.com/10.1002/2013JG002597> doi: 10.1002/2013JG002597
- Furniss, M., McGregor, M., Foiles, M., & Partridge, A. (1979). Chronology and characteristics of a Douglas-fir beetle outbreak in northern Idaho. USDA Forest Service General Technical Report INT-59. *Intermountain Forest and Range Experiment Station, Ogden, UT.*, 19.
- Geiszler, D., Gara, D., & Littke, W. (1984). Bark beetle infestations of lodgepole pine following a fire in south central Oregon. *Ztschrift fur Angewandte Entomologie*, 98(1-5), 389–394.
- Hansen, E., Bentz, B., & Turner, D. (2001). Temperature-based model for predicting univoltine brood proportions in spruce beetle (Coleoptera: Scolytidae). *Canadian Entomologist*, 133(6), 827–841.
- Hansen, E., Bentz, B. J., Powell, J. A., Gray, D. R., & Vandygriff, J. C. (2011, October). Prepupal diapause and instar IV developmental rates of the spruce beetle, *Dendroctonus rufipennis* (Coleoptera: Curculionidae, Scolytinae). *Journal of Insect Physiology*, 57(10), 1347–1357. Retrieved 2015-10-20, from <http://linkinghub.elsevier.com/retrieve/pii/S0022191011001892> doi: 10.1016/j.jinsphys.2011.06.011

- Hart, S., Veblen, T., & Kulakowski, D. (2014). Do tree and stand-level attributes determine susceptibility of spruce-fir forests to spruce beetle outbreak in the early 21st century? *Forest Ecology and Management*, 318, 44–53.
- Hood, S., & Bentz, B. (2007). Predicting postfire Douglas-fir beetle attacks and tree mortality in the northern Rocky Mountains. *Canadian Journal of Forest Research*, 37, 1058–1069.
- Jean, M., Mack, M., & Johnstone, J. (2017). *Murphy Dome: Moss (*Hylocomium splendens*) biomass results from a moss transplant and leaf litter manipulation experiment in three pairs of adjacent black spruce and birch stands*. Bonanza Creek LTER - University of Alaska Fairbanks: BNZ:671. Retrieved from <http://www.lter.uaf.edu/data/data-detail/id/671> (doi:10.6073/pasta/7df8bb07dbbd38f8eede86cff05be04)
- Johnstone, J., Hollingsworth, T., Chapin III, F., & Mack, M. (2010). Changes in fire regime break the legacy lock on successional trajectories in Alaskan boreal forest. *Global Change Biology*, 16(4), 1281–1295.
- Jumikis, A. (1966). *Thermal Soil Mechanics*. New Brunswick, NJ: Rutgers University Press.
- Kalkstein, L. (1976). Effects of climatic stress upon outbreaks of the southern pine beetle. *Environmental Entomology*, 5, 653–658.
- Keane, R., Loehman, R., & Holsinger, L. (2011). The FireBGCv2 Landscape Fire Succession Model: A research simulation platform for exploring fire and vegetation dynamics. *USDA Forest Service General Technical Report, RMRS-GTR-55*, 145.
- Keith, F., & Kreider, J. (1978). *Principles of Solar Engineering*. Washington, D.C.: Hemisphere.
- Klein, S. (1977). Calculation of monthly average insolation on tilted surfaces. *Solar Energy*, 19, 325–329.
- Larcher, W. (1980). *Physiological plant ecology*. Berlin: Springer-Verlag.
- Larsson, S., Oren, R., Waring, R., & Barrett, J. (1983). Attacks of mountain pine beetle as related to tree vigor of ponderosa pine. *Forest Science*, 29(2), 395–402.
- L'ecuyer, P. (1988). Efficient and portable combined random number generators. *Communications of the ACM*, 31(6).
- Leemans, R., & Prentice, I. (1989). *FORSKA, a general forest succession model*. Uppsala, Sweden: Institute of Ecological Botany.
- Liu, B., & Jordan, R. (1962). Daily insolation on surfaces tilted towards the equator. *American Society of Heating, Refrigerating, and Air-Conditioning Engineers*, 67, 526–541.

- Lunardini, V. (1981). *Heat Transfer in Cold Climates*. New York: Van Nostrand Reinhold.
- Malmstrom, C., & Raffa, K. (2000). Biotic disturbance agents in the boreal forest: considerations for vegetation change models. *Global Change Biology*, 6, 35–48.
- Mattson, W., & Haack, R. (1987). The role of drought in outbreaks of plant-eating insects. *Bioscience*, 37, 110–118.
- McKenzie, D., Peterson, D. L., & Littell, J. J. (2009). Chapter 15 Global Warming and Stress Complexes in Forests of Western North America. In *Developments in Environmental Science* (Vol. 8, pp. 319–337). Elsevier. Retrieved 2015-10-22, from <http://linkinghub.elsevier.com/retrieve/pii/S1474817708000156>
- Mezei, P., Grodzki, W., Blazenec, M., Skvarenina, J., Brandysova, V., & Jakus, R. (2014). Host and site factors affecting tree mortality caused by the spruce bark beetle (*Ips typographus*) in mountainous conditions. *Forest Ecology and Management*, 331, 196–207.
- Negron, J. (1998). Probability of infestation and extent of mortality associated with the Douglas-fir beetle in the Colorado Front Range. *Forest Ecology and Management*, 107, 71–85.
- Nicholls, R., & Child, T. (1979). Solar radiation charts. *Solar Energy*, 22(1).
- Oechel, W., & Van Cleve, K. (1986). The role of bryophytes in nutrient cycling in the taiga. In K. Van Cleve, F. Chapin, P. Flanagan, L. Viereck, & C. Dyrness (Eds.), *Forest ecosystems in the Alaskan taiga* (pp. 121–137). New York: Springer-Verlag.
- Parton, W., Schimel, D., Ojima, D., & Cole, C. (1994). A general model for soil organic matter dynamics: sensitivity to litter chemistry, texture and management. In R. Bryant & R. Arnold (Eds.), *Quantitative modeling of soil forming processes* (pp. 147–167). ASA, CSSA and SSA, Madison, Wisconsin: SSSA Spec. Publ. 35.
- Pastor, J., Gardner, R., Dale, V., & Post, W. (1987). Successional changes in nitrogen availability as a potential factor contributing to spruce declines in boreal North America. *Canadian Journal of Forest Research*, 17, 1394–1400.
- Pastor, J., & Post, W. (1984). Calculating Thornthwaite and Mather's actual evapotranspiration using an approximating function. *Canadian Journal of Forest Research*, 14, 466–467.
- Pastor, J., & Post, W. (1985). *Development of a linked forest productivity-soil process model* (Environmental Sciences Division Publication No. ORNL/TM-9519). Oak Ridge National Laboratory: USDA.
- Peet, R. K. (1981). Forest vegetation of the Colorado front range. *Vegetatio*, 45(1), 3–75. Retrieved 2015-10-23, from <http://link.springer.com/>

[article/10.1007/BF00240202](https://doi.org/10.1007/BF00240202)

- Press, W., Flannery, B., Teukolsky, S., & Vetterling, W. (1989). *Numerical Recipes in Pascal (First Edition): The Art of Scientific Computing* (1st ed.). Cambridge, UK: Cambridge University Press.
- Rasmussen, L., Amman, G., Vandygriff, J., Oakes, R., Munson, A., & Gibson, K. (1996). Bark beetle and wood borer infestation in the greater Yellowstone area during four postfire years. *USDA Forest Service Research Paper INT-RP-487. Intermountain Research Station, Ogden, UT*.
- Reicosky, D., Winkelman, L., Baker, J., & Baker, D. (1989). Accuracy of hourly air temperatures calculated from daily minima and maxima. *Agricultural and Forest Meteorology*, 46, 193–209.
- Rich, R., Frelich, L., & Reich, P. (2007). Wind-throw mortality in the southern boreal forest: effects of species, diameter and stand age. *Journal of Ecology*, 95, 1261–1273.
- Rosenberg, N., Blad, B., & Verma, S. (1983). *Microclimate*. New York: Wiley.
- Schmid, J. M., & Frye, R. H. (1976). *Stand ratings for spruce beetles* (Vol. 309). US Dept. of Agriculture, Forest Service, Rocky Mountain Forest and Range Experiment Station. Retrieved 2015-10-23, from http://books.google.com/books?hl=en&lr=&id=pddZMOAdeWOC&oi=fnd&dq=%22where+subalpine+fir+is+a+stand%22+%22of+trees+before+action+was+initiated.%22+%22ago,+it+is+unsatisfactory+today.+The+nation%22+%22Forester,+San+Juan+National+Forest,+Pagosa%22+&ots=183r56z_Ug&sig=EEr5jRHMFNU2EEC360azYP6XzLo
- Schmid, J. M., & Frye, R. H. (1977). *Spruce beetle in the Rockies* (General Technical Report No. RM-49). Fort Collins, CO: USDA Forest Service Rocky Mountain Research Station. Retrieved 2015-10-20, from <http://digitalcommons.usu.edu/barkbeetles/86/>
- Schumacher, S., Reineking, B., Sibold, J., & Bugmann, H. (2006). Modeling the impact of climate and vegetation on fire regimes in mountain landscapes. *Landscape Ecology*, 21, 539–554.
- Seidl, R., Baier, P., Rammer, W., Schopf, A., & Lexer, M. (2007). Modelling tree mortality by bark beetle infestation in Norway spruce forests. *Ecological Modelling*, 206(3-4), 383–399.
- Sherriff, R. L., Berg, E. E., & Miller, A. E. (2011). Climate variability and spruce beetle (*Dendroctonus rufipennis*) outbreaks in south-central and southwest Alaska. *Ecology*, 92(7), 1459–1470. Retrieved 2015-10-19, from <http://www.esajournals.org/doi/abs/10.1890/10-1118.1>
- Shinozaki, K., Yoda, K., Hozumi, K., & Kira, T. (1964). A quantitative anal-

- ysis of plant form - the pipe model theory. I. Basic analysis. *Japanese Journal of Ecology*, 14, 19–105.
- Shugart, H. (1984). *A Theory of Forest Dynamics: The Ecological Implications of Forest Succession Models*. New York, NY: Springer Science & Business Media.
- Shugart, H., & Seagle, S. (1985). Modeling forest landscapes and the role of disturbance in ecosystems and communities. In S. Pickett & P. White (Eds.), *The Ecology of Natural Disturbance and Patch Dynamics* (pp. 353–368). Elsevier.
- Shugart, H., Wang, B., Fischer, R., Ma, J., Fang, J., Yan, X., ... Armstrong, A. (2018). Gap models and their individual-based relatives in the assessment of the consequences of global change. *Environmental Research Letters*, 13(3). doi: 10.1088/1748-9326/aaaacc
- Shugart, H., & Woodward, F. (2011). *Global Change and the Terrestrial Biosphere*. Sussex, UK: Wiley-Blackwell.
- Shuman, J., Foster, A., Shugart, H., Hoffman-Hall, A., Krylov, A., Loboda, T., ... Sochilova, E. (2017). Fire disturbance and climate change: implications for Russian forests. *Environmental Research Letters*, 12. doi: 10.1088/1748-9326/aa5eed
- Singh, P., Kumar, N., & Arora, M. (2000). Degree-day factors for snow and ice for Dokriani Glacier, Garhwal Himalayas. *Journal of Hydrology*, 234(1-2), 1–11.
- Sturm, M., Taras, B., Liston, G., Derksen, C., Jonas, T., & Lea, J. (2010). Estimating snow water equivalent using snow depth data and climate classes. *Journal of Hydrometeorology*, 11, 1380–1394.
- Templer, C., Bugmann, H., & Elkin, C. (2013). Cross-scale interactions among bark beetles, climate change, and wind disturbances: a landscape modeling approach. *Ecological Monographs*, 83(3), 383–402.
- Van Cleve, K., Chapin, F., & Ruess, R. (2017). *Bonanza Creek LTER: Hourly Air Temperature Measurements (sample, min, max) at 50 cm and 150 cm from 1988 to Present in the Bonanza Creek Experimental Forest near Fairbanks, Alaska*. Bonanza Creek LTER - University of Alaska Fairbanks: BNZ:1. Retrieved from <http://www.lter.uaf.edu/data/data-detail/id/1> (doi:10.6073/pasta/006bae44c88f7d8b6fabe8cfebee86ff)
- Van Cleve, K., Oliver, L., Schlentner, R., Viereck, L., & Dyrness, C. (1983). Productivity and nutrient cycling in taiga forest ecosystems. *Canadian Journal of Forest Research*, 13, 747–766.
- Van Cleve, K., & Viereck, L. (1981). Forest succession in relation to nutrient cycling in the boreal forest of Alaska. In D. West, H. Shugart, & D. Botkin (Eds.), *Forest Succession. Concepts and Applications* (pp.

- 185–211). New York, NY.: Springer-Verlag.
- Veblen, T. T., Hadley, K. S., Nel, E. M., Kitzberger, T., Reid, M., & Villalba, R. (1994). Disturbance Regime and Disturbance Interactions in a Rocky Mountain Subalpine Forest. *The Journal of Ecology*, 82(1), 125. Retrieved 2015-10-20, from <http://www.jstor.org/stable/2261392?origin=crossref> doi: 10.2307/2261392
- Waring, R., & Pitman, G. (1980). *A simple model of host resistance to bark beetles* (Tech. Rep. No. RN-65). Corvallis, OR: Oregon State University, School of Forestry.
- Wichmann, L., & Ravn, H. P. (2001). The spread of Ips typographus (L.) (Coleoptera, Scolytidae) attacks following heavy windthrow in Denmark, analysed using GIS. *Forest Ecology and Management*, 148(1), 31–39. Retrieved 2015-10-20, from <http://www.sciencedirect.com/science/article/pii/S0378112700004771>
- Wigmsta, M., Vail, L., & Lettenmaier, D. (1994). A distributed hydrology-vegetation model for complex terrain. *Water Resources Research*, 30(6), 1665–1679.
- Yan, X., & Shugart, H. H. (2005, August). FAREAST: a forest gap model to simulate dynamics and patterns of eastern Eurasian forests: Simulation of eastern Eurasian forests. *Journal of Biogeography*, 32(9), 1641–1658. Retrieved 2015-10-20, from <http://doi.wiley.com/10.1111/j.1365-2699.2005.01293.x> doi: 10.1111/j.1365-2699.2005.01293.x
- Yarie, J., & Van Cleve, K. (1997). *Litterbag decomposition study, BCEF LTER sites, 1989-1997*. Bonanza Creek LTER - University of Alaska Fairbanks: BNZ:68. Retrieved from <http://www.lter.uaf.edu/data/data-detail/id/68>
- Zolubas, P., Negron, J., & Munson, A. (2009). Modelling spruce bark beetle infestation probability. *Baltic Forestry*, 15(1), 23–27.